extension at 72°C for 1 min. The PCR products were separated by electrophoresis on 2.0% agarose gels and visualized by staining with ethidium bromide.[1]

### *Adipogenic differentiation*

WJe-MSCs were cultured at $2\times10^4$ cells/well in six-well plates in α-MEM supplemented with 10% FBS. When the cells achieved 80% confluence, the medium was replaced with adipogenesis induction medium,[8] consisting of 100 μM indomethacin (Sigma–Aldrich), 1 μM dexamethasone (Sigma–Aldrich), 0.5 mM IBMX (Sigma–Aldrich), and 10 μg/mL insulin (Sigma–Aldrich). The medium was refreshed every 3 days. After 3 weeks, the cells were fixed with 10% formaldehyde, washed with PBS and 60% isopropanol, and stained with Oil Red O (Sigma–Aldrich).

### *Osteogenic differentiation*

WJe-MSCs at $2\times10^4$/well (P2) and SSEA4$^+$ and SSEA4$^-$ WJe-MSCs were cultured in 24-well plates in α-MEM supplemented with 10% FBS. On the following day, the medium was replaced with osteogenic induction medium including 10 nM dexamethasone (Sigma–Aldrich), 10 mM β-glycerol phosphate (Sigma–Aldrich), 100 μM ascorbic acid (Sigma–Aldrich), and 50 ng/mL human BMP2 (rhBMP2; Peprotech).[18,19] Human-BM-derived MSCs were used as the positive control. The induction medium was refreshed every 3 days. After 5 weeks, the cells were fixed with 2.5% glutaraldehyde for 15 min at room temperature followed by rinsing with PBS. The bone matrix was stained with 2% Alizarin Red S solution (Sigma–Aldrich) with pH adjusted to ~4.1–4.3 with 1% ammonium hydroxide (Sigma–Aldrich).[19]

### *Statistical analysis*

Differences between groups were analyzed with JMP 6.0.2 software (SAS Institute). Statistical analyses were performed with Turkey–Kramer tests, and a $p$-value of 0.05 was regarded as statistically significant.

## Results

### *Collection efficiency and WJe-MSC and WJc-MSC biomarkers*

Both WJe-MSCs and WJc-MSCs were spindle-shaped fibroblast-like cells (Fig. 1B). There was no significant difference between these two methods in the collected cell numbers at P0, even though the collected cell numbers of WJe-MSCs varied (Fig. 2A). The median number of collected WJe-MSCs from 1 g of WJ was $2\times10^6$ (range, from $9.1\times10^4$ to $10.3\times10^6$; $n=23$) and of collected WJc-MSCs was $1.7\times10^6$ (range, from $9.2\times10^4$ to $7.5\times10^6$; $n=20$). Further, we compared their surface markers as defined by the ISCT. Both WJe-MSCs and WJc-MSCs were positive for CD73, CD90, CD105, and HLA-ABC with a small percentage of cells also positive for CD271 and negative for CD34, CD45, and HLA-DR (Fig. 2B). In addition, both WJe-MSCs and WJc-MSCs expressed the ES-related genes *Nanog*, *Oct4*, *Klf4*, *Rex1*, and *Sox2* (Fig. 2C).

### *Expression of SSEA4 and SSEA3 in WJ-MSCs*

Because SSEA4$^+$ and SSEA3$^+$ cells have been considered as representative of immature cells, we periodically monitored SSEA4, SSEA3, and CD73 expression in WJe-MSCs and WJc-MSCs during P0–P9. The percentages of SSEA4$^+$ cells at P0 were similar in WJe-MSCs and WJc-MSCs. At P0, the WJe-MSCs included 32.4%±17.5% SSEA4$^+$CD73$^+$, 62.8%±18.9% SSEA4$^-$CD73$^+$, and 1.3%±1.8% SSEA4$^+$CD73$^-$, whereas the WJc-MSCs included 26.1%±16.1%, 70.4%±16.2%, and 0.7%±0.8% cells, respectively ($n=8$, $p=0.21$). However, the percentage of WJe-MSC SSEA4$^+$ cells decreased after the first passage and recovered to the original level by P7, whereas the incidence of WJc-MSC SSEA4$^+$ cells was relatively stable until P9 (Fig. 3A, C). In contrast, the percentage of SSEA3$^+$ cells among both WJe-MSCs and WJc-MSCs was highest at P0 that declined and disappeared by P5 (Fig. 3B, D). At P0, the percentage of SSEA3$^+$ cells among WJe-MSCs was 6.7%±6.3% and among WJc-MSCs was 6.1%±6.1% ($n=6$).

### *Comparison of SSEA4$^+$ and SSEA4$^-$ cells sorted from WJe-MSCs*

Further, we sorted SSEA4$^+$ and SSEA4$^-$ cells from WJe-MSCs at P4 using FACSAria and analyzed the SSEA4 expression in the sorted cells every week. The mean purity of SSEA4$^+$CD73$^+$ was 89% and that of SSEA4$^-$CD73$^+$ was 97.7%. The SSEA4$^+$ MSCs and SSEA4$^-$ MSCs were of similar sizes (Fig. 4A).

The percentage of SSEA4$^+$ cells derived from the sorted SSEA4$^+$ WJe-MSCs decreased rapidly in the first week and then increased gradually until week 4 (Fig. 4B, C). Interestingly, SSEA4$^+$ MSCs were present in the SSEA4$^-$ WJe-MSCs, and the incidence of SSEA4$^+$ cells in the subsequent cultures was similar to that in the SSEA4$^+$-sorted cells. After week 4, the incidence of SSEA4$^+$ cells from both the SSEA4$^+$ and SSEA4$^-$ MSCs decreased to <10%. The incidences of SSEA4$^+$ cells derived from SSEA4$^+$ WJe-MSCs and SSEA4$^-$ WJe-MSCs were 8.5%±8.8% and 8.5%±8.8% at week 1 and 43.5%±21.6% and 55.1%±29.4% at week 4, respectively ($n=3$; Fig. 4C). In addition, there was no difference in proliferation ability between SSEA4$^+$ and SSEA4$^-$ WJe-MSCs (Fig. 4D).

RT-PCR analysis showed that the sorted SSEA4$^+$ and SSEA4$^-$ WJe-MSCs expressed *Nanog*, *Oct4*, and *Klf4* (Fig. 4E).

### *Adipocyte differentiation*

To determine the differentiation ability of SSEA4$^+$ WJe-MSCs, we induced sorted SSEA4$^+$ and SSEA4$^-$ WJe-MSCs into adipocytes. With induction medium, we observed the accumulation of Oil Red O-stained lipid drops in SSEA4$^+$, SSEA4$^-$, and nonsorted WJe-MSCs, whereas there were no changes in WJe-MSCs cultured without induction medium (Fig. 5A).

### *Osteogenic differentiation*

We also compared the osteogenic differentiation abilities of SSEA4$^+$ and SSEA4$^-$ WJe-MSCs. There was no difference between SSEA4$^+$ and SSEA4$^-$ WJe-MSCs after histochemical staining with Alizarin red, even though WJe-MSCs were difficult to differentiate into osteoblasts, as previously reported. Induction of osteogenic differentiation in WJe-MSCs required a relatively high concentration

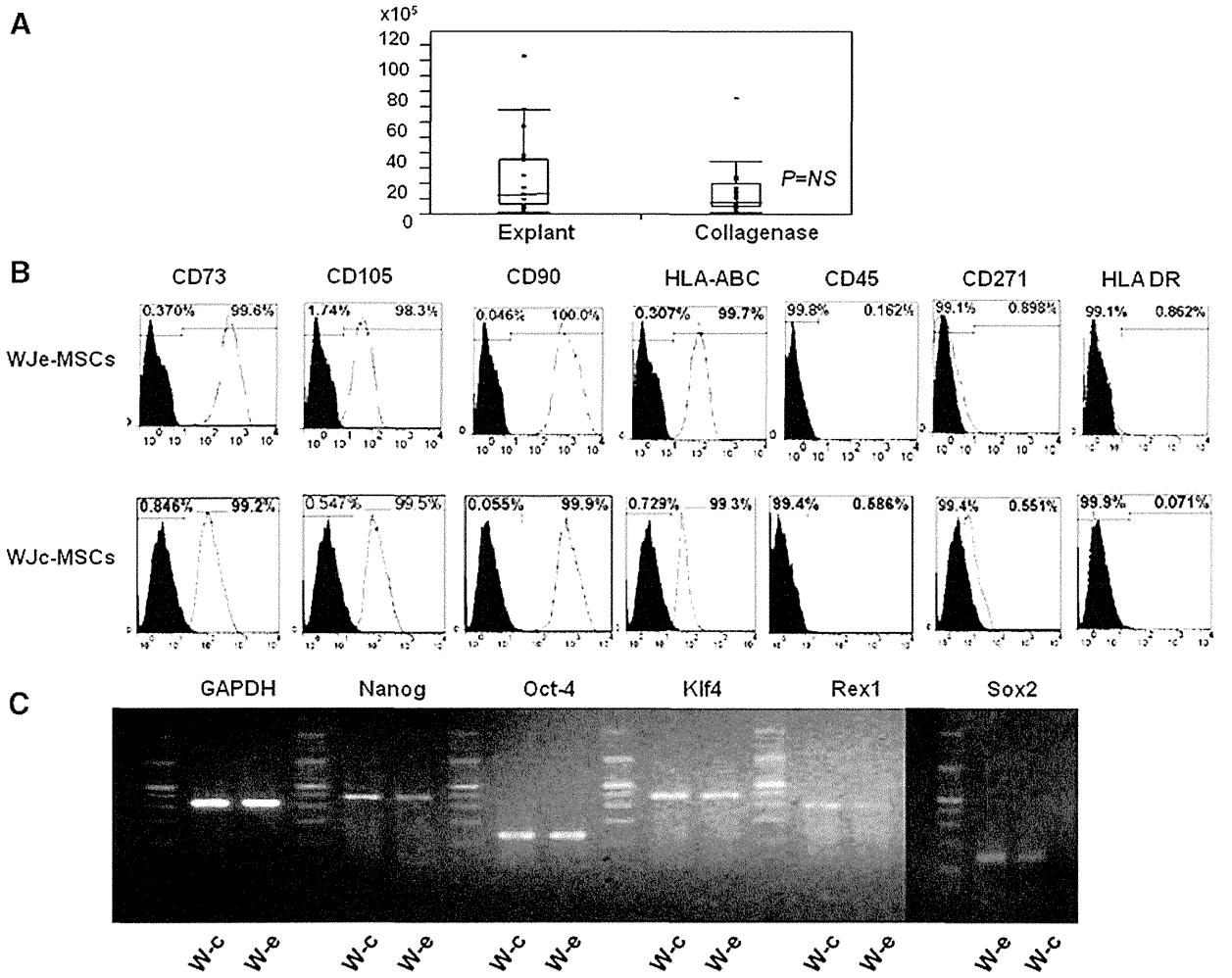


**FIG. 2.** Characterization of WJ-MSCs collected by the explant and the collagenase-treatment methods. **(A)** Median cell numbers of WJ-MSCs collected by the explant method ($n=23$) and the collagenase-treatment method are shown ($n=20$). **(B)** Both WJe-MSCs and WJc-MSCs were positive for CD73, CD90, CD105, CD271, and HLA class I and negative for CD45 and HLA class II. **(C)** Expression of embryonic stem cell–related markers *Nanog*, *Oct4*, *Klf4*, *Rex1*, and *Sox2* is shown. The data are representative of three individual experiments.

(100 nM/mL) of BMP2 and a longer culture period of 5 weeks ($n=3$; Fig. 5B).

### *Expression of SSEA4/3 in media with different FBS concentrations*

We examined SSEA4/3 expression after 1 week in cultures containing 0.1%, 1%, 10%, and 20% FBS, which contains GSL. The cultured WJe-MSCs were all positive for CD73, and cell proliferation of WJe-MSCs was associated with FBS concentration (Fig. 6A, B). The SSEA4 expression was positively correlated with the FBS concentration (Fig. 6C), whereas SSEA3 expression was negatively correlated (Fig. 6D). The WJe-MSCs were $15.8\% \pm 6.2\%$ $SSEA4^+CD73^+$ and $5.8\% \pm 1.9\%$ $SSEA3^+CD73^+$ in 0.1% FBS medium, $24.5\% \pm 9.8\%$ and $2.7\% \pm 1.0\%$ in 1% FBS, $41.5\% \pm 13.1\%$ and $0.7\% \pm 0.5\%$ in 10% FBS, and $48.3\% \pm 12.0\%$ and $0.6\% \pm 0.4\%$ in 20% FBS, respectively ($n=3$).

To see that the increase in SSEA4 expression upon increasing FBS concentration is caused by the change in expression alone but not because of increased WJe-MSC proliferation, we analyzed SSEA4 expression associated with growth curve with different FBS concentrations. In consistent with the prior data, SSEA4 expression was correlated with FBS concentration, while SSEA3 was inversely correlated (Fig. 6E–G). The higher FBS concentration accelerated the proliferation of WJe-MSCs with higher expression of SSEA4 (Fig. 6E, F). The incidence of $SSEA4^+$ and $SSEA3^+$ cells was highest on day 3, followed by the decline from days 3 to 7, still during proliferation. The possibility of the substrate shortage for SSEA4 and SSEA3 during culture could be denied, because we replaced the fresh medium on day 4. The data are representative of three individual experiments.

Next, when the sorted $SSEA4^+$ and $SSEA4^-$ WJe-MSCs were cultured in 1%, 5%, and 10% FBS for 1 week, SSEA4

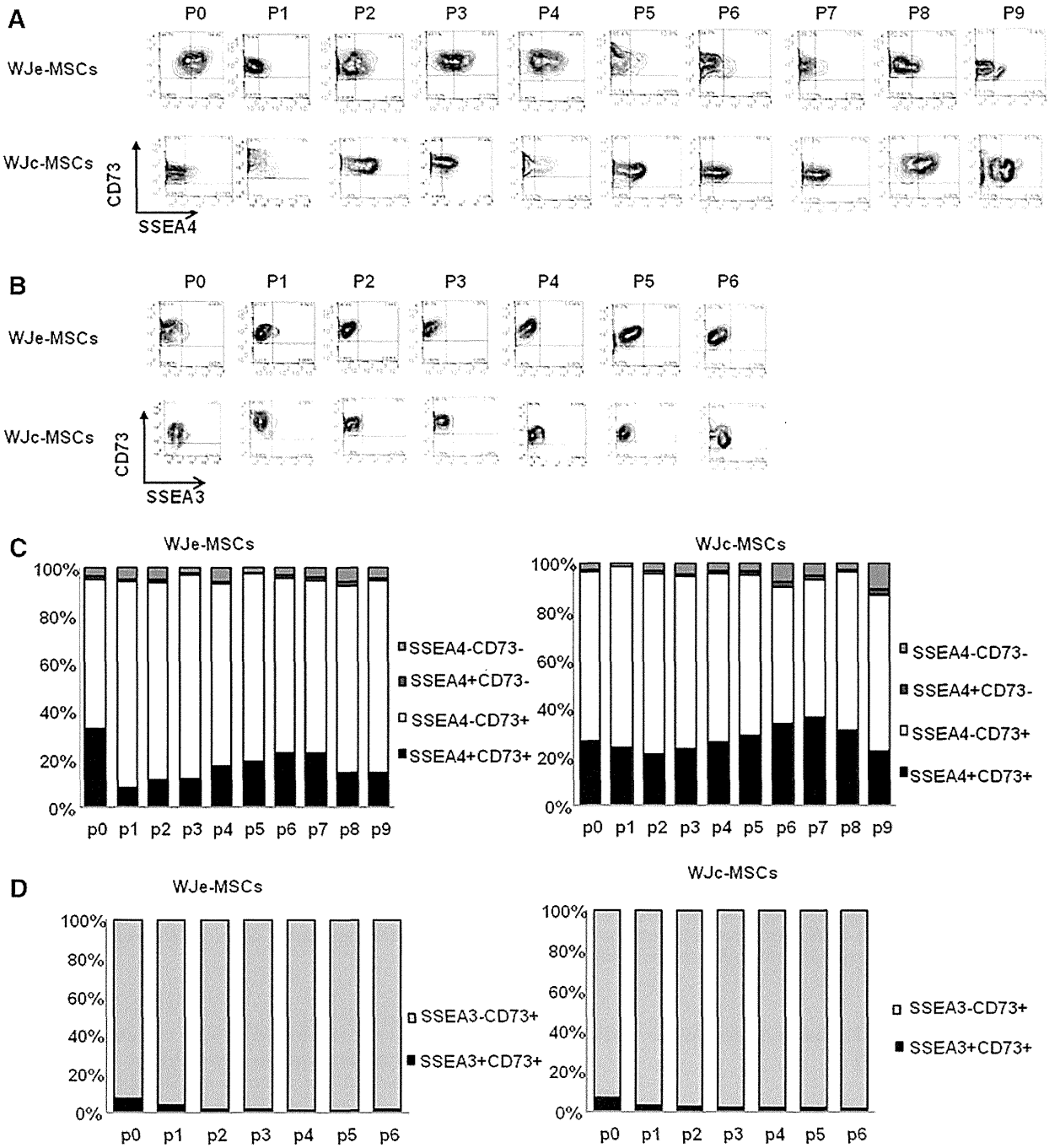


**FIG. 3.** Stage-specific embryonic antigen-4 expression during passages. **(A)** Stage-specific embryonic antigen 4 (SSEA4) and CD73 expression was monitored in WJ-MSCs collected by the explant (WJe-MSCs) and the collagenase-treatment methods (WJc-MSCs) during P0–P9. **(B)** SSEA3 and CD73 expression was periodically monitored in WJe-MSCs and WJc-MSCs during P0–P6. **(C)** The mean incidence of SSEA4 and CD73 in WJe-MSCs and WJc-MSCs is shown. **(D)** The mean incidence of SSEA3 in $CD73^+$ WJe-MSCs and WJc-MSCs is shown. The data are representative of eight individual experiments.

expression in the sorted $SSEA4^+$ WJe-MSCs was 4.74% and 17.4% in 1% and 10% FBS medium, respectively, whereas SSEA4 expression in the sorted $SSEA4^-$ WJe-MSCs was 2.69% and 5.08% in 1% and 10% FBS, respectively ($n=3$; Fig. 6H, I).

Further, to clarify whether the phenomena of SSEA4 expression influenced by FBS concentration were limited to WJe-MSCs, we performed the same experiments using BM-MSCs derived from frozen-thawed MNCs. As shown in Figure 7A, BM-MNCs before culture included hematopoietic

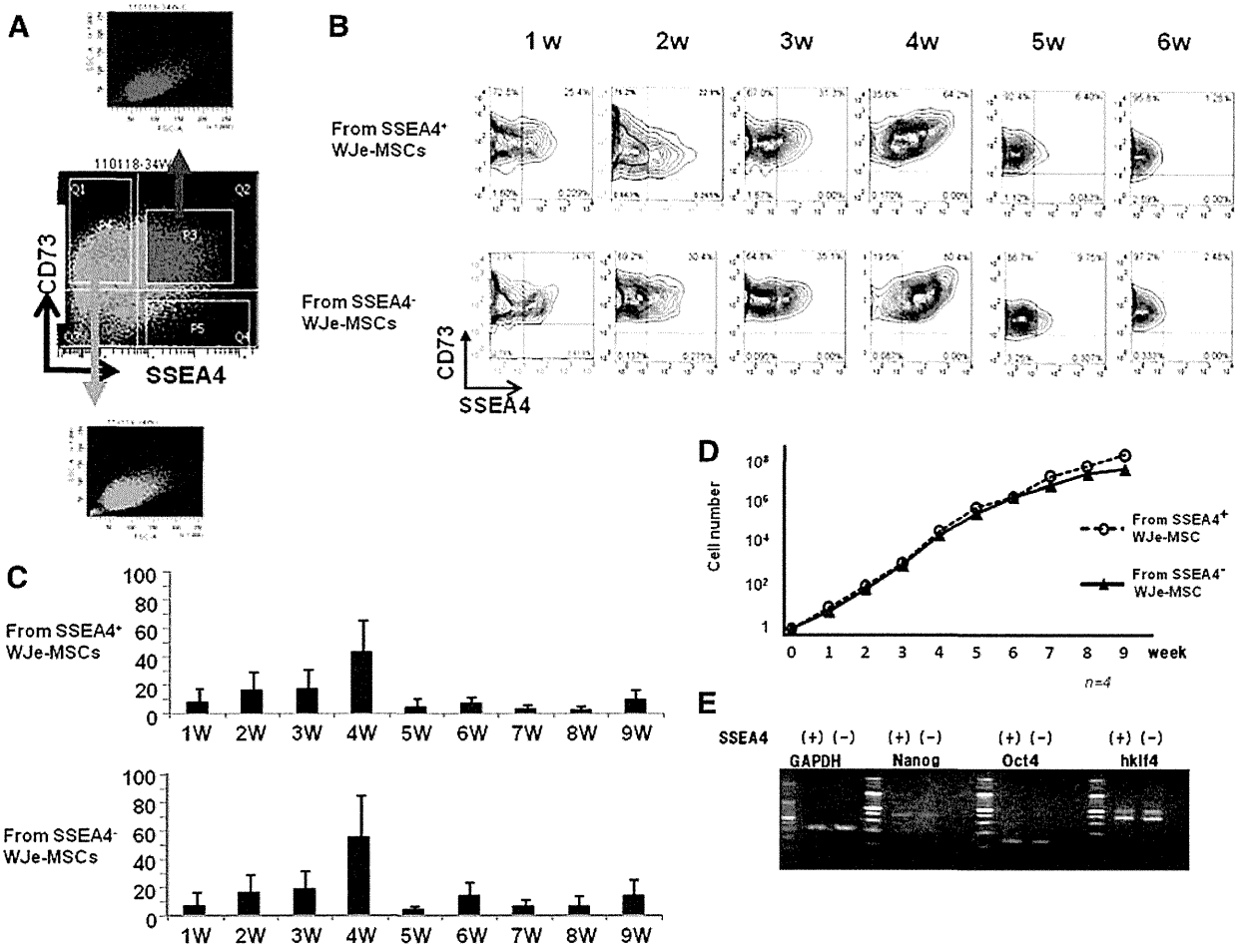


**FIG. 4.** Sorted SSEA4$^+$ and SSEA4$^-$ WJ-MSCs collected by the explant method. **(A)** SSEA4$^+$CD73$^+$ WJ-MSCs and SSEA4$^-$CD73$^+$ WJe-MSCs were sorted by FACSAria. **(B)** SSEA4 and CD73 expression in sorted SSEA4$^+$ and SSEA4$^-$ WJe-MSCs during passages 1–6 weeks (w) is shown. **(C)** The percentages of SSEA4$^+$ cells in the sorted SSEA4$^+$ and SSEA4$^-$ WJe-MSCs during weeks 1–9 are shown ($n=3$). **(D)** Growth curves of the sorted SSEA4$^+$ (open circles) and SSEA4$^-$ (closed triangles) WJe-MSCs over 9 weeks are shown. **(E)** Gene expression analysis of the sorted SSEA4$^+$ and SSEA4$^-$ WJe-MSCs showed that both were positive for *Oct4*, *Nanog*, and *Klf4*. Color images available online at www.liebertpub.com/tea

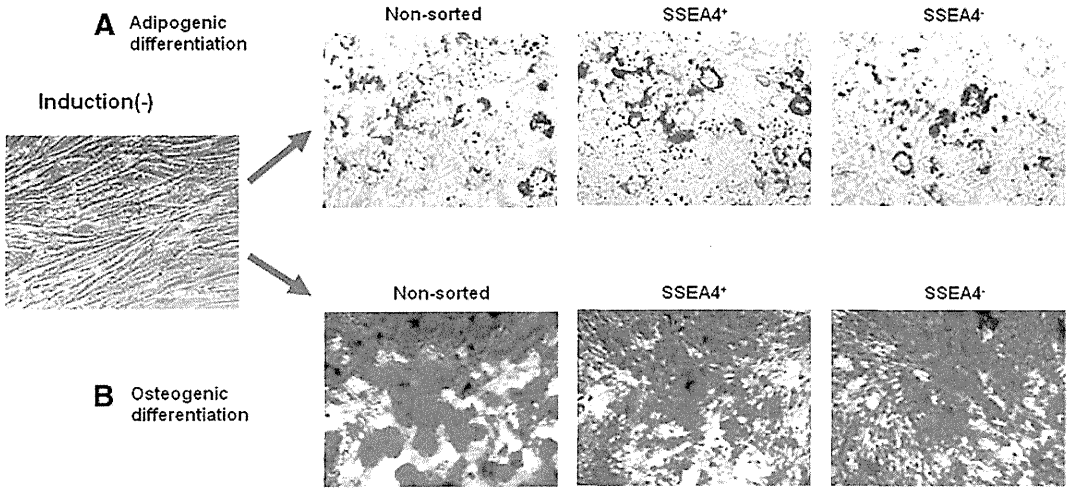


**FIG. 5.** Adipogenic and osteogenic differentiation of sorted SSEA4$^+$ and SSEA4$^-$ WJ-MSCs. **(A)** Adipogenic differentiation of nonsorted and SSEA4$^+$- and SSEA4$^-$-sorted WJe-MSCs is shown by Red O-stained lipid drops at 3 weeks. **(B)** Osteogenic differentiation of unsorted and SSEA4$^+$- and SSEA4$^-$-sorted WJe-MSCs is shown. Color images available online at www.liebertpub.com/tea

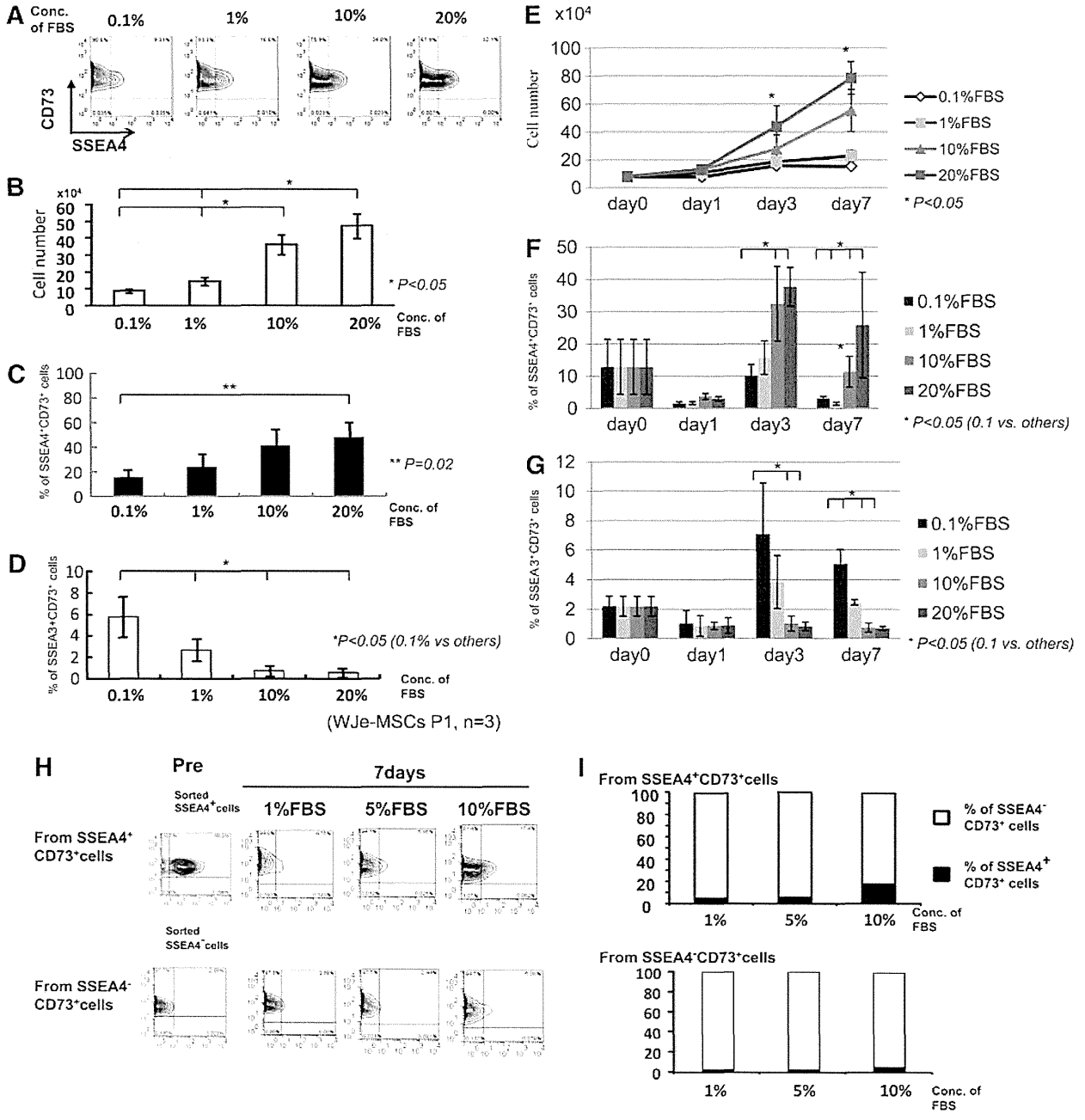


**FIG. 6.** Influence of fetal bovine serum (FBS) on SSEA4 and SSEA3 expression. **(A)** WJ-MSCs collected by the explant method (WJe-MSCs) were cultured for 1 week in media containing 0.1%, 1%, 10%, and 20% FBS, and SSEA4 expression patterns were analyzed by flow cytometry. The data are representative of three individual experiments. **(B)** WJe-MSC numbers in media with different concentrations of FBS were determined. **(C, D)** Percentages of $SSEA4^+$ and $SSEA3^+$ cells, respectively, among the WJe-MSCs in media with different concentrations of FBS were determined. **(E)** Growth curves of WJe-MSCs with different concentrations of FBS. **(F, G)** Percentage of $SSEA4^+$ and $SSEA3^+$ cells during the proliferation of WJe-MSCs, respectively. **(H, I)** Flow cytometry patterns and percentages of SSEA4 expression in the sorted $SSEA4^+$ and $SSEA4^-$ WJe-MSCs in media with 1%, 5%, and 10% FBS were determined. $^*P<0.05$, $^{**}P=0.02$.

cells with low incidence of MSCs and also low incidence of SSEA4+cells. As expected, the proportion of $CD45^+$ hematopoietic cell expression declined during the passages; instead, $CD45^-$ cells increased (Fig. 7A). The latter cells expressed $CD45^-CD73^+$ MSCs (data not shown). However, in α-MEM with 10% FBS, we could not observe the predominant growth of $SSEA4^+$ cells regardless of CD45 expression (Fig. 7A). Further, in consistent with the results in WJ-MSCs, the SSEA4 expression in BM-MSCs was correlated with the FBS concentration, whereas SSEA3

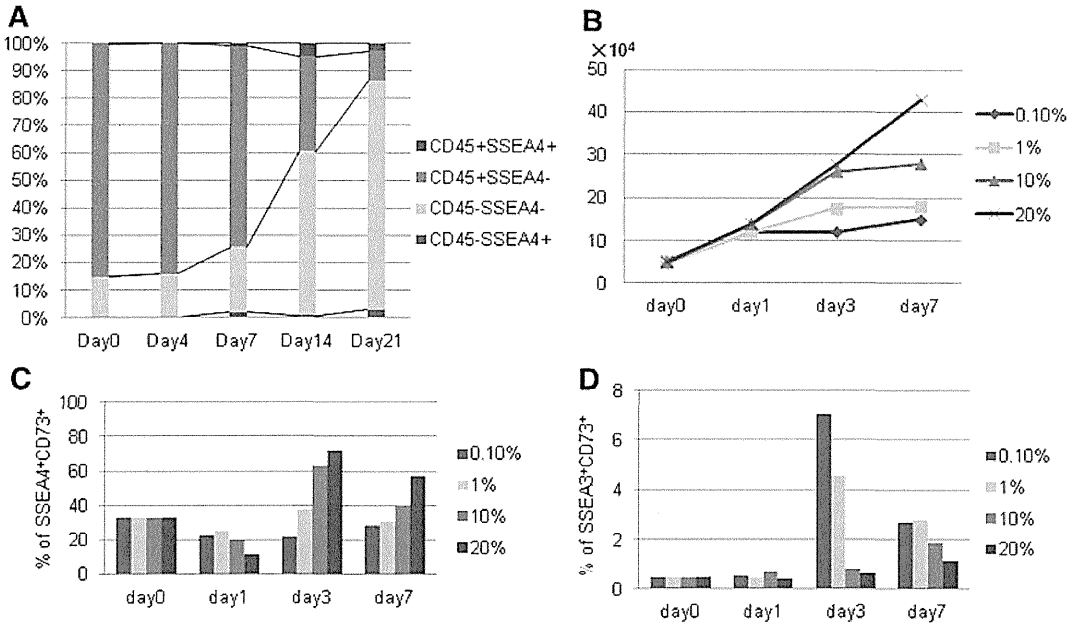


**FIG. 7.** Influence of FBS on SSEA4 and SSEA3 expression in bone-marrow-derived mesenchymal stem cells. **(A)** Shift of the proportion of $CD45^+$ hematopoietic cells and $CD45^-$ cells with or without SSEA4 expression during the passages. **(B)** Growth curves of BM-MSCs with different concentrations of FBS. **(C, D)** Percentage of $SSEA4^+$ and $SSEA3^+$ cells during the proliferation of BM-MSCs, respectively. The data are representative of two individual experiments.

expression was inversely correlated (Fig. 7B–D). The relationship between the growth curve and SSEA4/3 expression was also consistent with the results in WJ-MSCs (Figs. 6E–G and 7B–D).

## Discussion

To gain insight into the role of SSEA3 and SSEA4 in UC WJ-MSCs, we examined the SSEA3 and SSEA4 expression on WJ-MSCs obtained by different methods and compared the differentiation abilities of $SSEA4^+$ and $SSEA4^-$ cells.

First, we compared SSEA3 and SSEA4 expression in WJe-MSCs and WJc-MSCs. The explant method has several advantages. It does not require nonhuman collagenase derived from *Clostridium histolyticum* and saves the time for lysing the tissue with enzyme in the procedure. The disadvantages of the explant method are that collecting adequate cell numbers is dependent on the amount of WJ tissue fragments that attach firmly to the bottom of the dish, which in turn, is dependent on the individual ability. Although the collagenase process from cutting tissue to plating can be unified, we found that some samples are more sensitive to collagenase, resulting in reduced viability. We did not find any significant differences between WJe-MSCs and WJc-MSCs in cell numbers, MSC surface markers as defined by the ISCT, or ES-cell-related gene expression at P0. In addition, the incidence of $SSEA4^+$ and $SSEA3^+$ at P0 was similar between the two types. However, SSEA3 disappeared rapidly in the early culture passages, as described previously.[14,20] It is known that SSEA3 disappears more rapidly from the cell surface compared with SSEA4, if GSL synthesis is blocked by inhibitors, and a similar phenomenon has also been detected during ES cell differentiation.[14,21] Interestingly, the incidence of WJe-MSC $SSEA4^+$ cells was reduced after the first passage, and, by P7, the original levels were recovered. In contrast, the incidence of WJc-MSC $SSEA4^+$ cells was relatively stable until P9. The reason for the depression of SSEA4 expression in WJe-MSCs at P1 is unknown. However, $SSEA4^+$ MSCs in both WJe-MSCs and WJc-MSCs did not proliferate predominantly in our culture medium. As previously reported, osteogenic differentiation was difficult with WJ-MSCs,[8] requiring a longer induction period, additional cytokines such as BMP2, and specific FBS concentrations. However, both sorted $SSEA4^+$ and $SSEA4^-$ WJ-MSCs eventually differentiated into osteocytes and adipocytes in a similar manner, and there were no differences in ES-marker gene expression between the $SSEA4^+$ and $SSEA4^-$ MSCs. Interestingly, $SSEA4^+$ cells appeared even from the $SSEA4^-$ MSCs, and the incidence of $SSEA4^+$ cells derived from the $SSEA4^-$ MSCs demonstrated a similar transition pattern as those derived from the $SSEA4^+$ MSCs. This result suggested that the culture medium may have been the source of SSEA4 antigens.

The role of SSEA3 and SSEA4 in MSCs remains controversial. Rostovskaya *et al.* also suggested SSEA4-marked adipogenic progenitor lacking osteogenic capacity.[22] In ES cell study, Ramirez *et al.* demonstrated that both SSEA3 and SSEA4 are markers of immature ES cells, but particularly SSEA3 together with OCT4 and TRA-1–60 were good tracers for validating pluripotent stem cells, whereas SSEA4 was expressed for long during the differentiation of ES cells.[20] Gang *et al.* reported that $SSEA4^+$ cells proliferated predominantly when the culture was initiated from primary BM cells, which were mostly hematopoietic cells.[11] But in our culture condition, the incidence of $SSEA4^+$ cells, which were characterized as MSCs, was not increased dramatically

as reported by Gang's group. Their results might be induced by the special cocktail of the medium, consisted of MCDB-201, 10% FBS, ITS, linoleic acid–bovine serum albumin, dexamethasone, ascorbic acid, hPDGF-BB, and hEGF, followed by the medium with relatively high FBS concentration. In other articles, Schrobback *et al.* assessed the SSEA4 in human articular chondrocytes, osteoblasts, and BM-derived MSCs and characterized their differentiation potential. But their results showed that SSEA4 levels in these cells were not unrelated to the cells' chondrogenic and osteogenic and proliferation potentials *in vitro*.[23] Suila *et al.* reported that SSEA4, and not SSEA3, was expressed on the surface of cord-blood-derived MSCs, whereas SSEA3 was expressed at very low levels in cord blood hematopoietic stem cells.[24] They also suggested that FBS contains detectable amounts of globoseries GSLs and showed that the SSEA3 was influenced and upregulated by culturing with FBS overnight, even though they did not demonstrate an influence on SSEA4 expression. In our study, we demonstrated that SSEA4 expression significantly correlated with FBS concentration, whereas SSEA3 appeared to be negatively correlated with FBS concentration. The possibility that FBS stimulated the proliferation of WJe-MSCs, resulting in the increase of SSEA4 expression, cannot be denied completely. But the fact that the SSEA4 expression was declined during the proliferation of WJe-MSCs and BM-MSCs in each medium did not support this hypothesis. Regardless of cell growth or cell concentration, consistently, the SSEA4 expression was clearly associated with FBS concentration not only in WJ-MSCs but also in BM-MSCs. Reversely to the SSEA4 expression, SSEA3 expression appeared to be negatively correlated with FBS concentration. The reason why the data of SSEA3 elevation upon the higher FBS concentration are not coincident with Suila's data remained unresolved. We add a partial speculation that SSEA4 is derived from SSEA3; thus, the increase of SSEA4 means the waste of SSEA3, or MSCs with high concentration of FBS are differentiated accompanied with decrease of SSEA3. But we need the scrupulous attention to analyze SSEA3 by FCM in various FBS concentrations. We also found that SSEA4 could be induced from pure $SSEA4^-$ WJ-MSCs. This suggests the presence of substrate for SSEA4 in $SSEA4^-$ cells and also the influence of FBS on the SSEA4 expression in $SSEA4^-$ cells. Brimble *et al.* reported that the depletion of these two molecules by the addition of GSL synthesis inhibitors apparently did not affect the ES cell pluripotency.[14] In conclusion, these results indicate that SSEA4 may display altered expression profiles in response to culture medium including FBS and may not be an essential marker of WJ-MSC pluripotency.

## Acknowledgments

This study was supported by the Ministry of Health, Labor and Welfare, Japan, and the Ministry of Education, Culture, Sports, Science and Technology, Japan. We thank Mr. Tomoki Tamura and Ms. Yukiko Enomoto for their technical support. The authors would like to thank Enago (www.enago.jp) for the English language review.

## Disclosure Statement

The authors have no conflicts of interest.

## References

1. Ishige, I., Nagamura-Inoue, T., Honda, M.J., Harnprasopwat, R., Kido, M., Sugimoto, M., *et al.* Comparison of mesenchymal stem cells derived from arterial, venous, and Wharton's jelly explants of human umbilical cord. Int J Hematol **90,** 261, 2009.
2. Kode, J.A., Mukherjee, S., Joglekar, M.V., and Hardikar, A.A. Mesenchymal stem cells: immunobiology and role in immunomodulation and tissue regeneration. Cytotherapy **11,** 377, 2009.
3. Zeddou, M., Briquet, A., Relic, B., Josse, C., Malaise, M.G., Gothot, A., *et al.* The umbilical cord matrix is a better source of mesenchymal stem cells (MSC) than the umbilical cord blood. Cell Biol Int **34,** 693, 2010.
4. Horwitz, E.M., Le Blanc, K., Dominici, M., Mueller, I., Slaper-Cortenbach, I., Marini, F.C., *et al.* Clarification of the nomenclature for MSC: The International Society for Cellular Therapy position statement. Cytotherapy **7,** 393, 2005.
5. Dominici, M., Le Blanc, K., Mueller, I., Slaper-Cortenbach, I., Marini, F., Krause, D., *et al.* Minimal criteria for defining multipotent mesenchymal stromal cells. The International Society for Cellular Therapy position statement. Cytotherapy **8,** 315, 2006.
6. Anzalone, R., Iacono, M.L., Corrao, S., Magno, F., Loria, T., Cappello, F., *et al.* New emerging potentials for human Wharton's jelly mesenchymal stem cells: immunological features and hepatocyte-like differentiative capacity. Stem Cells Dev **19,** 423, 2010.
7. Carvalho, M.M., Teixeira, F.G., Reis, R.L., Sousa, N., and Salgado, A.J. Mesenchymal stem cells in the umbilical cord: phenotypic characterization, secretome and applications in central nervous system regenerative medicine. Curr Stem Cell Res Ther **6,** 221, 2011.
8. Hsieh, J.Y., Fu, Y.S., Chang, S.J., Tsuang, Y.H., and Wang, H.W. Functional module analysis reveals differential osteogenic and stemness potentials in human mesenchymal stem cells from bone marrow and Wharton's jelly of umbilical cord. Stem Cells Dev **19,** 1895, 2010.
9. Fong, C.Y., Chak, L.L., Biswas, A., Tan, J.H., Gauthaman, K., Chan, W.K., *et al.* Human Wharton's jelly stem cells have unique transcriptome profiles compared to human embryonic stem cells and other mesenchymal stem cells. Stem Cell Rev **7,** 1, 2011.
10. Kannagi, R., Cochran, N.A., Ishigami, F., Hakomori, S., Andrews, P.W., Knowles, B.B., *et al.* Stage-specific embryonic antigens (SSEA-3 and -4) are epitopes of a unique globo-series ganglioside isolated from human teratocarcinoma cells. EMBO J **2,** 2355, 1983.
11. Gang, E.J., Bosnakovski, D., Figueiredo, C.A., Visser, J.W., and Perlingeiro, R.C. SSEA-4 identifies mesenchymal stem cells from bone marrow. Blood **109,** 1743, 2007.
12. Kuroda, Y., Kitada, M., Wakao, S., Nishikawa, K., Tanimura, Y., Makinoshima, H., *et al.* Unique multipotent cells in adult human mesenchymal cell populations. Proc Natl Acad Sci USA **107,** 8639, 2010.
13. Wakao, S., Kitada, M., Kuroda, Y., and Dezawa, M. Isolation of adult human pluripotent stem cells from mesenchymal cell populations and their application to liver damages. Methods Mol Biol **826,** 89, 2012.
14. Brimble, S.N. Sherrer, E.S., Uhl, E.W., Wang, E., Kelly, S., Merrill, A.H. Jr., Robins, A.J., and Schulz, T.C. The cell surface glycosphingolipids SSEA-3 and SSEA-4 are not essential for human ESC pluripotency. Stem Cells **25,** 54, 2007.

15. Tong, C.K., Vellasamy, S., Tan, B.C., Abdullah, M., Vidyadaran, S., Seow, H.F., *et al.* Generation of mesenchymal stem cell from human umbilical cord tissue using a combination enzymatic and mechanical disassociation method. Cell Biol Int **35,** 221, 2011.
16. Lee, K.S., Nah, J.J., Lee, B.C., Lee, H.T., Lee, H.S., So, B.J., *et al.* Maintenance and characterization of multipotent mesenchymal stem cells isolated from canine umbilical cord matrix by collagenase digestion. Res Vet Sci **94,** 144, 2013.
17. Takahashi, K., Tanabe, K., Ohnuki, M., Narita, M., Ichisaka, T., Tomoda, K., *et al.* Induction of pluripotent stem cells from adult human fibroblasts by defined factors. Cell **131,** 861, 2007.
18. Wulsten, D., Glatt, V., Ellinghaus, A., Schmidt-Bleek, K., Petersen, A., Schell, H., *et al.* Time kinetics of bone defect healing in response to BMP-2 and GDF-5 characterised by *in vivo* biomechanics. Eur Cells Mater **21,** 177, 2011.
19. Agata, H., Asahina, I., Watanabe, N., Ishii, Y., Kubo, N., Ohshima, S., *et al.* Characteristic change and loss of *in vivo* osteogenic abilities of human bone marrow stromal cells during passage. Tissue Eng Part A **16,** 663, 2010.
20. Ramirez, J.M., Gerbal-Chaloin, S., Milhavet, O., Qiang, B., Becker, F., Assou, S., *et al.* Brief report: benchmarking human pluripotent stem cell markers during differentiation into the three germ layers unveils a striking heterogeneity: all markers are not equal. Stem Cells **29,** 1469, 2011.
21. Draper, J.S., Pigott, C., Thomson, J.A., and Andrews, P.W. Surface antigens of human embryonic stem cells: changes upon differentiation in culture. J Anat **200,** 249, 2002.
22. Rostovskaya, M., and Anastassiadis, K. Differential expression of surface markers in mouse bone marrow mesenchymal stromal cell subpopulations with distinct lineage commitment. PloS One **7,** e51221, 2012.
23. Schrobback, K., Wrobel, J., Hutmacher, D.W., Woodfield, T.B., and Klein, T.J. Stage-specific embryonic antigen-4 is not a marker for chondrogenic and osteogenic potential in cultured chondrocytes and mesenchymal progenitor cells. Tissue Eng Part A **19,** 1316, 2013.
24. Suila, H., Pitkanen, V., Hirvonen, T., Heiskanen, A., Anderson, H., Laitinen, A., *et al.* Are globoseries glycosphingolipids SSEA-3 and -4 markers for stem cells derived from human umbilical cord blood? J Mol Cell Biol **3,** 99, 2011.

Address correspondence to:
*Tokiko Nagamura-Inoue, MD, PhD*
*Department of Cell Processing and Transfusion*
*The Institute of Medical Science*
*The University of Tokyo*
*4-6-1Shirokanedai, Minato-ku*
*Tokyo 108-8639*
*Japan*

*E-mail:* tokikoni@ims.u-tokyo.ac.jp

*Received: June 4, 2013*
*Accepted: November 12, 2013*
*Online Publication Date: March 12, 2014*

Brief Report

LYMPHOID NEOPLASIA

# In vivo leukemogenic potential of an interleukin 7 receptor α chain mutant in hematopoietic stem and progenitor cells

Kazuaki Yokoyama,[1,2] Nozomi Yokoyama,[3] Kiyoko Izawa,[1] Ai Kotani,[4] Akira Harashima,[5] Katsuto Hozumi,[2] and Arinobu Tojo[1]

[1]Division of Molecular Therapy, Advanced Clinical Research Center, Institute of Medical Science, University of Tokyo, Tokyo, Japan; [3]Department of Laboratory Medicine, Research Hospital, Institute of Medical Science, University of Tokyo, Tokyo, Japan; [2]Department of Immunology and [4]Institute of Innovation Science and Technology, Tokai University School of Medicine, Kanagawa, Japan; and [5]Cell Biology Institute, Research Center, Hayashibara Biochemical Laboratories, Okayama, Japan

**Key Points**

- Gain-of function mutation of IL7Rα induces lymphoid leukemia as well as myeloproliferative disease.
- In vivo oncogenicity of mutant IL7Rα is influenced by the differentiation stage at which it occurs.

**Somatic gain-of-function mutations in interleukin 7 receptor α chain (IL7Rα) have been described in pediatric T and B acute lymphoblastic leukemias (T/B-ALLs). Most of these mutations are in-frame insertions in the extracellular juxtamembrane-transmembrane region. By using a similar mutant, a heterozygous in-frame transmembrane insertional mutation (INS), we validated leukemogenic potential in murine hematopoietic stem/progenitor cells, using a syngeneic transplantation model. We found that ectopic expression of INS alone in hematopoietic stem/progenitor cells caused myeloproliferative disorders, whereas expression of INS in combination with a Notch1 mutant led to the development of much more aggressive T-ALL than with wild-type IL7Rα. Furthermore, forced expression of INS in common lymphoid progenitors led to the development of mature B-cell ALL/lymphoma. These results demonstrated that INS has significant in vivo leukemogenic activity and that the lineage of the resulting leukemia depends on the developmental stage in which INS occurs, and/or concurrent mutations. (*Blood.* 2013;122(26):4259-4263)**

## Introduction

Interleukin 7 (IL7) is essential for T-cell development and homeostasis.[1] Its cognate receptor (IL7R) forms a heterodimer composed of the α chain (IL7Rα) and common γ chain; binding of IL7 to IL7R triggers activation of Janus kinase (JAK)/signal transducer and activator of transcription signaling and the PI3K/v-akt murine thymoma viral oncogene homolog 1 (Akt) pathways.[1]

Accumulating evidence has demonstrated that dysregulation of the IL7 signaling axis may be implicated in lymphoid malignancies. For example, IL7 transgenic mice develop T- and B-cell lymphomas,[1] and human primary T-cell acute lymphoblastic leukemia (T-ALL) cells respond to IL7 in vitro[1] and in vivo.[2] Moreover, recent findings describing IL7Rα gain-of-function mutations in pediatric ALL and a T-ALL cell line have provided direct evidence that the IL7-IL7R axis plays a crucial role in the pathogenesis of human ALL.[3-6]

Although the gain-of-function properties of these mutants have been precisely studied in vitro,[3-5] their leukemogenic potential in vivo has not been well studied. One study reported that T-cell leukemogenesis was triggered by an IL7Rα mutant.[5] However, they used murine IL7-dependent D1 progenitor T-cell lines derived from p53-knockout mice,[7] which spontaneously develop T-cell lymphoma,[8,9] and this specific animal model may not be generally applicable.

To extend these observations, we demonstrate the in vivo leukemogenic potential of such a mutant when expressed in primary hematopoietic stem and progenitor cells by using a IL7Rα mutant, which was previously identified in a T-ALL cell line.[6]

## Methods

### Mice

Six- to 12-week-old Balb/c mice were used for all experiments. Lineage depletion of bone marrow (BM) or embryonic day 14.5 (E14.5) fetal liver was performed by the EasySep Mouse Hematopoietic/Progenitor Cell Enrichment Kit (StemCell Technologies). Via tail vein injection, $1 \times 10^6$ Lineage$^-$ BM/fetal liver cells (lin$^-$ cells), pro-B, or Thy1$^+$T cell progenitors were injected into lethally (8 Gy) or sublethally (4 Gy) irradiated recipients. Mice were maintained in accordance with institutional animal care guidelines (Institute of Medical Science, University of Tokyo). Detailed methods are provided in the supplemental Methods.

Submitted August 20, 2012; accepted October 10, 2013. Prepublished online as *Blood* First Edition paper, October 30, 2013; DOI 10.1182/blood-2012-08-451278.

K.Y. and N.Y. contributed equally to this study.

The online version of this article contains a data supplement.

There is an Inside *Blood* commentary on this article in this issue.

The publication costs of this article were defrayed in part by page charge payment. Therefore, and solely to indicate this fact, this article is hereby marked "advertisement" in accordance with 18 USC section 1734.

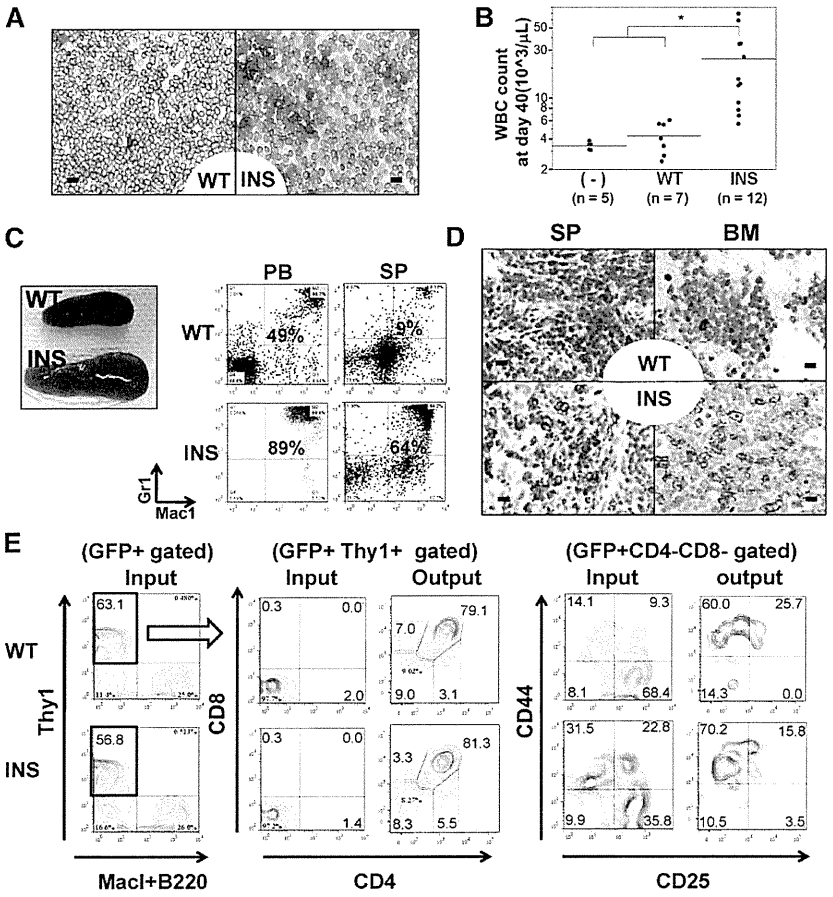


**Figure 1. In vivo transforming activity of INS.** (A-D) Lin$^-$ cells were retrovirally transduced with mock vectors (mock), WT, or INS, followed by injection into lethally irradiated congenic mice. (A) May-Giemsa staining of PB smears at day 40, showing marked leukocytosis consisting predominantly of mature myeloid cells. (B) White blood cell count at day 40. *$P < .05$ (analysis of variance; INS vs WT or mock recipient mice). (C) FACS of the PB and SP at day 40, showing an increase in Mac-1$^+$/Gr-1$^+$ myeloid cells. (D) Immunohistochemical analysis (IHC) of SP and BM specimens by anti-myeloperoxidase, indicating an increase in the number of myeloid cells in INS recipient mice. Bars represent (A) 10 μm and (D) 20 μm. (E) Demonstration of in vivo reconstitutive capacity of hIL7R (WT/INS) transduced T-cell progenitors. Lin$^-$ kit$^+$ stem/progenitor cells were cultured on OP9-DL1 stromal layer for 7days, supplemented with mIL7$^+$ human Fms-like tyrosine kinase 3-ligand, which allowed them to differentiate into Thy1$^+$CD25$^-$CD44$^+$DN1 immature T-cell progenitor fractions. These cells were retrovirally transduced with WT/INS vector. The resultant cells were allowed to expand on OP9-DL1 stroma for additional 7 to 10 days, and developed into CD25$^+$CD44$^-$ DN3 immature T-cell progenitor fractions. These Thy1$^+$ cells were green fluorescent protein (GFP)-sorted and intravenously injected into sublethally irradiated mice. The resultant GFP$^+$ thymic seeding progenitors (denoted as "input") in recipient mice of WT and INS at day 52 was shown (denoted as "output").

## Results and discussion

### In vitro transforming activity of the mutant IL7Rα, INS

Consistent with previous report, sequencing analysis of exon 6 of the IL7Rα gene, mainly encoding the transmembrane domain, identified a heterozygous in-frame transmembrane insertional mutation (INS) in the T-ALL cell line DND-41.[6] Forced expression of INS exerted transforming activity in Ba/F3 cells, as revealed by acquisition of cytokine-independent growth (supplemental Figure 1A-C, found on the *Blood* website) as well as the autonomous phosphorylation of Stat1, Stat3, Stat5, and Akt (supplemental Figure 1D). In addition, transient expression of IL7Rα in human embryonic kidney 293 cells leads to autonomous tyrosine phosphorylation of Jak1 only in those expressing INS (supplemental Figure 1D, *left*), suggesting that INS constitutively activated IL7R downstream signals via Jak1. As INS falls within the same category of reported mutation of IL7Rα,[3-6] we decided to use INS as a representative gain-of-function IL7Rα mutation for further experiments.

### INS in stem/progenitor cells caused myeloproliferative disorders

The leukemogenic activity of INS and wild-type (WT) IL7Rα was assessed by retroviral transduction of Lin$^-$ cels. Within 6 to 9 weeks after transplantation, recipient mice transplanted with INS Lin$^-$ cells, but not WT Lin$^-$ cells, developed myeloproliferative disorders (MPDs) characterized by splenomegaly, leukocytosis, and polycythemia (Figure 1A-C, *right*; supplemental Figures 1D and 3C-D). Fluorescence-activated cell sorter (FACS) and morphological analysis revealed a marked increase in Mac1$^{++}$ Gr-1$^{++}$ mature myeloid cells in the peripheral blood (PB), spleen (SP), and BM (Figure 1C-D; supplemental Figures 2 and 4). An increase of Ter119$^+$ CD71$^+$ immature erythroblast was also noted in SP and BM (supplemental Figure 4, SP; data not shown). INS-induced MPD was oligoclonal, as evidenced by Southern blot analysis (supplemental Figure 5, *left*). A similar disease phenotype was also observed in mice transplanted with Lin$^-$c-Kit$^{++}$Sca1$^{++}$ (KSL) fractions transduced with INS (supplemental Figures 3A-B,E and 4). Both B- and T-cell development were severely perturbed in INS recipient mice (supplemental Figure 4). As transplantation of INS-transduced KSL cells resulted in preferential expansion of myeloid progenitor–enriched Lin$^-$c-Kit$^{++}$Sca1$^-$ fraction (supplemental Figure 6), we speculate that in vitro transforming activity of INS skewed myeloid progenitor expansion at the expense of common lymphoid progenitor Lin–c-kit$^{low}$Sca1$^+$ IL7Rα$^+$ (CLP) expansion, through which normal lymphopoiesis might be perturbed. This was also supported by the fact that INS exerted transforming activity in input KSL cells, as well as resultant myeloid progenitors ex vivo, as revealed by colony-forming cell assay (supplemental Figure 7). It was previously reported that forced expression of wild-type murine IL7Rα into IL7Rα knockout BM progenitors induces a very similar MPD phenotype, including

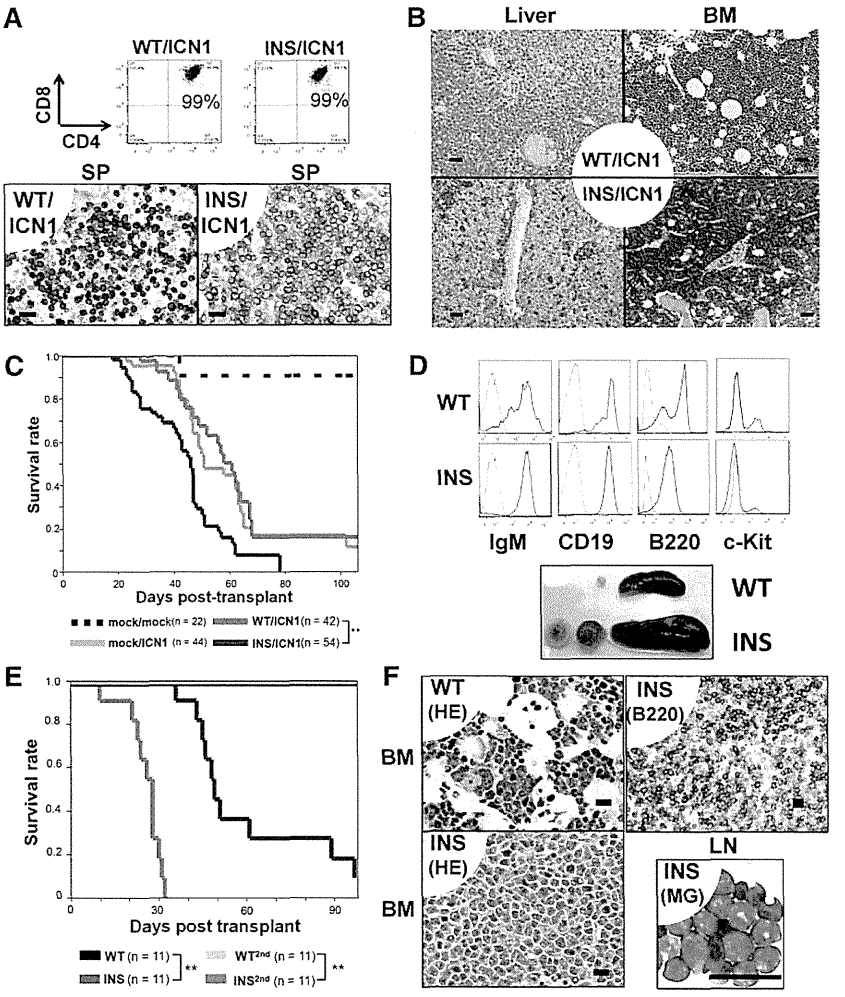


**Figure 2. INS synergized with active Notch1 (A-C) and exerted transforming activity in CLPs (D-F) in vivo.** (A-C) Lin$^-$ cells were cotransfected with vectors encoding the ICN1 gene (mock, ICN1) and the hIL7R gene (mock, WT, INS), followed by injection into lethally irradiated congenic mice. (A, *upper*) FACS analysis of the SP from WT/ICN1 or INS/ICN1 recipient mice at day 40. Data were obtained from GFP$^+$ (marker for the ICN1 gene) and rat CD2$^+$ (marker for the hIL7R gene) fractions. (A, *lower*) IHC of SP specimens using anti-CD3 antibodies from WT/ICN1 (*left*) and INS/ICN1 (*right*) recipient mice. Bar represents 20 μm. (B) Histological findings of liver (*left 2 panels*) and BM (*right 2 panels*) from WT/ICN1 (*upper*) and INS/ICN1 (*lower*) recipient mice (hematoxylin and eosin stain). Bar represents 50 μm. (C) Survival curves of recipient mice (mock/mock, n = 22; mock/ICN1, n = 44; WT/ICN1, n = 42; INS/ICN1, n = 54) $^{**}P < .01$ (log-rank test). (D-F) CLPs transfected with hIL7R constructs were expanded in vitro for 18 days and injected into sublethally irradiated congenic mice. (D, *top 2 panels*) FACS analysis of the BM: WT recipient mice at day 60 (WT) and INS recipient mice at day 60 (INS). Data are obtained from GFP$^+$ gated fractions. Open histogram, isotype control; shaded histogram, specific staining. (D, *lower*) Splenomegaly and lymphadenopathy developed in CLPs-INS recipient mice at day 60 (denoted as "INS"). (E) Survival curves of recipient mice (n = 11 for each condition). $^{**}P < .01$ (log-rank test, INS vs WT or INS vs INS$^{2nd}$). (F) Histological findings: BM specimens from WT recipient mice (*upper left*) and INS recipient mice at day 60 by hematoxylin and eosin stain (*lower left*) or by IHC of B220$^+$ cells (*upper right*). Lymph node cytospin from INS recipient mice at day 60 by May-Giemsa stain (*lower right*). Bar represents 20 μm. WT, WT primary recipients; INS, INS primary recipients; WT-2nd, WT day 30 BM secondary recipients; INS-2nd, INS day 30 BM secondary recipients.

splenomegaly resulting from neutrophilia.[10] Consistent with this report, transduced WT appeared to induce some degree of increase in myeloid fraction and neutrophilia in PB and SP compared with that of mock increase of myeloid fraction and neutrophilia in PB (supplemental Figure 4). Importantly, the magnitude was quite different, as we could not find a statistically significant difference of SP weight in mock and WT (n = 4 each; $P = .61$, 1-way analysis of variance; supplemental Figure 3C). This is in contrast to the difference of INS (n = 4) and WT ($P < .01$; supplemental Figure 3C). WT-induced mild myeloid expansion was accompanied by concomitant increase in lymphoid subset in PB, SP, and BM, specifically CD19$^+$ B-cell fractions (supplemental Figure 4). Considering the fact that the phenotype of WT-recipient mice was different from that of mock (supplemental Figure 4), it should be mentioned that we could not rule out the possibility that the phenotype elicited by INS is in part a result of the effect of IL7R overexpression per se, irrespective of its mutational status. The major difference from the previous report was that they rescued the loss-of-function phenotype of IL7Rα by ectopic expression of IL7Rα.[10]

Neither of these recipient mice developed overt leukemia throughout the median follow-up period of 5 months (WT, n = 28; INS, n = 22), suggesting that additional transforming events are required for clonal evolution to aggressive leukemia. Considering the fact that recipient mice for hematopoietic stem cells transduced with constitutively active Akt or signal transducer and activator of transcription-5 also developed similar diseases together,[11,12] this MPD phenotype is likely to be induced by stem cells ectopically expressing INS.

### Nononcogenic consequence of INS in T-cell progenitors

Next, we wished to test the effect of INS on T-cell precursors. Toward this aim, we cocultured Lin$^-$ kit$^+$ stem/progenitor cells for 7 days, which allowed the emergence of Thy1$^+$CD25$^-$CD44$^+$DN1 immature T-cell-progenitor fractions (data not shown). These cells were transduced by retroviral transduction of the WT/INS vector. The resultant transduced cells were allowed to expand on OP9 expressing the Notch ligand Delta-like 1 (OP9-DL1) stroma for an additional 7 to 10 days, which allowed them to develop Thy1$^+$ CD4$^-$CD8$^-$CD25$^-$CD44$^+$DN1 to DN3 CD25$^+$CD44$^-$DN3 immature T-cell-progenitor fractions (Figure 1E). The resultant Thy1$^+$ cells were GFP sorted and injected into sublethally irradiated mice. As a result, we could detect stable engraftment of GFP$^+$ T-cell progenitors in recipient mice from day 40 to day 50 in thymus (Figure 1E) and CD4 or CD8 single-positive cells in the periphery, such as SP or PB (data not shown). Neither of these recipient mice

developed overt leukemia throughout the median follow-up period of 106 days (WT and INS, n = 12 each). We speculate that this might be partly attributable to the limited engraftment of WT/INS-transduced T-cell progenitors in thymus (data not shown).

### INS exacerbates the in vivo oncogenic activity of Notch1

INS-like mutations were reported to occur in 10% of T-ALL patients.[3,4] In contrast, Notch1 mutations were more frequently found in T-ALL patients and were equally distributed between patients with WT and INS.[4,] The DND-41 cell line carries both INS and Notch1 mutations.[6,13] Moreover, IL7 signaling coordinates with Notch1 in proper T-cell developmental programming.[14,15] We hypothesized that INS may cooperate with active Notch1 mutants in T-cell leukemogenesis. Therefore, $Lin^-$ cells were transduced with mock or IL7Rα-WT/INS along with an active form of intracellular Notch1 (ICN1), followed by syngeneic transplantation. As reported previously,[16] within 4 to 6 weeks after transplantation, all mice developed T-ALL, characterized by extrathymic expansion of leukemic cells (Figure 2A-B; supplemental Figure 8B). Clonality of INS/ICN1-induced leukemia was confirmed by Southern blot analysis around day 35 (supplemental Figure 5, *right*). Despite similar immunophenotypes ($CD3^+CD4^+CD8^+TCR\text{-}\beta^+$) between WT/ICN1 and INS/ICN1 cells (Figure 2A, *Upper*; supplemental Figures 8A and 9), histological examinations of the liver, SP, and BM in recipient mice revealed that systemic expansion of INS/ICN1-$Lin^-$ cells was much more aggressive than that of WT/$ICN1^-$ and mock/$ICN1^-Lin^-$ cells (Figure 2A, *Lower*, and 2B). Furthermore, the median survival time of INS/ICN1 mice (44 days; n = 54) was significantly shorter than that of mock/ICN1 (60 days; n = 44) and WT/ICN1 (57 days; n = 42) mice ($P < .001$ by log-rank test; Figure 2C). Taken together, INS clearly exaggerated ICN1-induced T-ALL.

### Forced expression of INS in B-cell progenitors caused mature B-ALL/lymphoma

Because the IL7Rα gene is transcriptionally active in common lymphoid progenitors (CLPs; $Lin^-c\text{-}kit^{low}Sca1^+$ $IL7R\alpha^+$) and their progenies and not expressed in stem cell compartments,[17] the INS allele could target the same cell populations. Then, CLPs were transduced with INS or WT IL7Rα and cultured on the OP9 stromal layer with a cytokine cocktail for 18 days, followed by transplantation of resulting pro-B cells into syngeneic recipient mice (supplemental Figure 10A). All but 1 of the INS-CLP recipients died of mature B-ALL/lymphoma, whereas no WT-CLP recipients died ($P < .01$; Figure 2D-E). Autopsy specimens revealed massive infiltration of $B220^+$ leukemic blasts into the BM, SP, and lymph nodes (Figure 2F; data not shown). This mature B-cell ALL/lymphoma was transplantable to secondary recipients, resulting in more aggressive mature B-ALL/lymphoma with much shorter survival periods (Figure 2E). INS-induced mature B-ALL/lymphoma was biclonal, as evidenced by Southern blot analysis (supplemental Figure 5, *right*). Under these experimental conditions, INS-CLPs had already committed to the cytokine-independent clonogenic pro-B cells before transplantation (supplemental Figure 10B-C; data not shown).

Finally, we wished to identify the downstream signals involved in INS-induced leukemogenesis. Using microarray analysis (Gene Expression Omnibus accession number GSE51211) of the resultant transformed cells in vitro and in vivo, we performed a comparative analysis of gene expression profiles from WT and INS-transduced hematopoietic stem/progenitor cells, as well as resultant leukemia cells that developed in vivo. As a result, we found a list of candidate genes (n = 6133) that were up- or downregulated by INS in comparison with WT. Among those genes, by reviewing hierarchical clustering analysis, several genes could be candidate mediators downstream of INS in comparison with WT, including hairy and enhancer of split-1 (*HES1*) for MPD, proviral insertion site in Moloney murine leukemia virus 1 (*PIM1*) for B-ALL, and insulin-like growth factor 1 receptor (*IGF1R*) for T-ALL (supplemental Figure 11). Quantitative RT-PCR verified their differential expression in comparison with WT (supplemental Figure 12). Putative involvement of these genes in INS-induced leukemogenesis was supported by previous data reporting the significance of *HES1* overexpression reported in advanced chronic myelogenous leukemia,[18] *PIM1* activation involved in pre-B-cell transformation,[19] *PIM1* overexpression reported in B-ALL,[20] and high-level expression of *IGF1R* in T-ALL.[20,21] In addition, we performed gene set enrichment analysis[22] to find significant overlaps between INS/ICN1 (in comparison with WT/ICN1) gene expression signature and gene sets present in the public database (supplemental Discussion). As a result, we found that in vivo INS/ICN1 was characterized by overexpression of interferon (IFN)-stimulated genes[23] and IGF1-signal-related genes,[24] suggesting constitutive activation of $IFN^-$ as well as the $IGF1^-$ signal pathway (supplemental Figures 13 and 14; supplemental Tables 2 and 3). These are consistent with the previous report that JAK1-mutated T-ALL samples were characterized by the IFN-pathway[23] signature, as well as our findings of a higher *IGF1R* transcript level in INS/ICN1 cells compared with that of WT/ICN1 (supplemental Figures 11 and 12).

In conclusion, we provided evidence that INS has significant in vivo leukemogenic activity and that determination of the lineage of resulting leukemias depends on the developmental stage during which they occur and/or concurrent mutations. In addition, as far as we know, this is the first report in which transformation of CLP leading to in vivo malignancy is shown. This is also of general relevance for the field of lymphoid malignancies. Given that either IL7Rα or Jak1 gain-of-function mutations have been found in approximately 10%[3-5] or 19%[25] of T-ALL patients and that IFN-pathway signatures have been associated with Jak1-mutated T-ALL,[23] it is fairly certain that IFN-pathway signatures induced by aberrant IL7R/Jak1 axis might substantially contribute to the pathogenesis of T-ALL in close association with activating mutations in the Notch pathways.

## Acknowledgment

We thank Kana Minegishi and Kazuo Ogami for their help.

## Authorship

Contribution: K.Y., N.Y., and K.I. performed experiments; K.Y. wrote the manuscript; A.H., A.K., and K.H. provided vital reagents; and A.T. supervised the research.

Conflict-of interest disclosure: The authors declare no competing financial interests.

Correspondence: Arinobu Tojo, Department of Hematology-Oncology, Research Hospital, Institute of Medical Science, the University of Tokyo, 4-6-1 Shirokanedai, Minato-ku, Tokyo 108-8639, Japan; e-mail: a-tojo@ims.u-tokyo.ac.jp.

## References


1. Barata JT, Cardoso AA, Boussiotis VA. Interleukin-7 in T-cell acute lymphoblastic leukemia: an extrinsic factor supporting leukemogenesis? *Leuk Lymphoma.* 2005;46(4): 483-495.
2. Silva A, Laranjeira AB, Martins LR, et al. IL-7 contributes to the progression of human T-cell acute lymphoblastic leukemias. *Cancer Res.* 2011;71(14):4780-4789.
3. Shochat C, Tal N, Bandapalli OR, et al. Gain-of-function mutations in interleukin-7 receptor-α (IL7R) in childhood acute lymphoblastic leukemias. *J Exp Med.* 2011;208(5):901-908.
4. Zenatti PP, Ribeiro D, Li W, et al. Oncogenic IL7R gain-of-function mutations in childhood T-cell acute lymphoblastic leukemia. *Nat Genet.* 2011; 43(10):932-939.
5. Zhang J, Ding L, Holmfeldt L, et al. The genetic basis of early T-cell precursor acute lymphoblastic leukaemia. *Nature.* 2012;481(7380):157-163.
6. Porcu M, Kleppe M, Gianfelici V, et al. Mutation of the receptor tyrosine phosphatase PTPRC (CD45) in T-cell acute lymphoblastic leukemia. *Blood.* 2012;119(19):4476-4479.
7. Kim K, Khaled AR, Reynolds D, Young HA, Lee CK, Durum SK. Characterization of an interleukin-7-dependent thymic cell line derived from a p53 (-/-) mouse. *J Immunol Methods.* 2003;274(1-2): 177-184.
8. Harvey M, McArthur MJ, Montgomery CA Jr, Butel JS, Bradley A, Donehower LA. Spontaneous and carcinogen-induced tumorigenesis in p53-deficient mice. *Nat Genet.* 1993;5(3):225-229.
9. Haines BB, Ryu CJ, Chang S, et al. Block of T cell development in P53-deficient mice accelerates development of lymphomas with characteristic RAG-dependent cytogenetic alterations. *Cancer Cell.* 2006;9(2):109-120.
10. Jiang Q, Li WQ, Aiello FB, Klarmann KD, Keller JR, Durum SK. Retroviral transduction of IL-7Ralpha into IL-7Ralpha-/- bone marrow progenitors: correction of lymphoid deficiency and induction of neutrophilia. *Gene Ther.* 2005;12(24): 1761-1768.
11. Kharas MG, Okabe R, Ganis JJ, et al. Constitutively active AKT depletes hematopoietic stem cells and induces leukemia in mice. *Blood.* 2010;115(7):1406-1415.
12. Kato Y, Iwama A, Tadokoro Y, et al. Selective activation of STAT5 unveils its role in stem cell self-renewal in normal and leukemic hematopoiesis. *J Exp Med.* 2005;202(1):169-179.
13. Weng AP, Ferrando AA, Lee W, et al. Activating mutations of NOTCH1 in human T cell acute lymphoblastic leukemia. *Science.* 2004; 306(5694):269-271.
14. Magri M, Yatim A, Benne C, et al. Notch ligands potentiate IL-7-driven proliferation and survival of human thymocyte precursors. *Eur J Immunol.* 2009;39(5):1231-1240.
15. García-Peydró M, de Yébenes VG, Toribio ML. Notch1 and IL-7 receptor interplay maintains proliferation of human thymic progenitors while suppressing non-T cell fates. *J Immunol.* 2006; 177(6):3711-3720.
16. Pear WS, Aster JC, Scott ML, et al. Exclusive development of T cell neoplasms in mice transplanted with bone marrow expressing activated Notch alleles. *J Exp Med.* 1996;183(5): 2283-2291.
17. Miller JP, Izon D, DeMuth W, Gerstein R, Bhandoola A, Allman D. The earliest step in B lineage differentiation from common lymphoid progenitors is critically dependent upon interleukin 7. *J Exp Med.* 2002;196(5):705-711.
18. Nakahara F, Sakata-Yanagimoto M, Komeno Y, et al. Hes1 immortalizes committed progenitors and plays a role in blast crisis transition in chronic myelogenous leukemia. *Blood.* 2010;115(14): 2872-2881.
19. Guo G, Qiu X, Wang S, et al. Oncogenic E17K mutation in the pleckstrin homology domain of AKT1 promotes v-Abl-mediated pre-B-cell transformation and survival of Pim-deficient cells. *Oncogene.* 2010;29(26): 3845-3853.
20. Haferlach T, Kohlmann A, Wieczorek L, et al. Clinical utility of microarray-based gene expression profiling in the diagnosis and subclassification of leukemia: report from the International Microarray Innovations in Leukemia Study Group. *J Clin Oncol.* 2010;28(15): 2529-2537.
21. Medyouf H, Gusscott S, Wang H, et al. High-level IGF1R expression is required for leukemia-initiating cell activity in T-ALL and is supported by Notch signaling. *J Exp Med.* 2011;208(9): 1809-1822.
22. Subramanian A, Tamayo P, Mootha VK, et al. Gene set enrichment analysis: a knowledge-based approach for interpreting genome-wide expression profiles. *Proc Natl Acad Sci USA.* 2005;102(43):15545-15550.
23. Hornakova T, Chiaretti S, Lemaire MM, et al. ALL-associated JAK1 mutations confer hypersensitivity to the antiproliferative effect of type I interferon. *Blood.* 2010;115(16): 3287-3295.
24. Creighton CJ, Casa A, Lazard Z, et al. Insulin-like growth factor-I activates gene transcription programs strongly associated with poor breast cancer prognosis. *J Clin Oncol.* 2008;26(25): 4078-4085.
25. Flex E, Petrangeli V, Stella L, et al. Somatically acquired JAK1 mutations in adult acute lymphoblastic leukemia. *J Exp Med.* 2008;205(4): 751-758.

# Histone demethylase Jmjd3 is required for the development of subsets of retinal bipolar cells

Atsumi Iida[a], Toshiro Iwagawa[a], Hiroshi Kuribayashi[a], Shinya Satoh[a], Yujin Mochizuki[a,b], Yukihiro Baba[a], Hiromitsu Nakauchi[c], Takahisa Furukawa[d], Haruhiko Koseki[e], Akira Murakami[b], and Sumiko Watanabe[a,1]

[a]Division of Molecular and Developmental Biology, Institute of Medical Science, University of Tokyo, Tokyo 108-8639, Japan; [b]Department of Ophthalmology, Juntendo University School of Medicine, Tokyo 113-8421, Japan; [c]Division of Stem Cell Therapy, Center for Stem Cell Biology and Regenerative Medicine, Institute of Medical Science, University of Tokyo, Tokyo 108-8639, Japan; [d]Laboratory for Molecular and Developmental Biology, Institute for Protein Research, Osaka University, Osaka 565-8871, Japan; and [e]Laboratory for Developmental Genetics, RIKEN Center for Allergy and Immunology, Kanagawa 230-0045, Japan

Edited by Seth Blackshaw, Johns Hopkins University School of Medicine, Baltimore, MD, and accepted by the Editorial Board January 30, 2014 (received for review June 24, 2013)

**Di- and trimethylation of lysine 27 on histone H3 (H3K27me2/3) is an important gene repression mechanism. H3K27me2/3-specific demethylase, Jmjd3, was expressed in the inner nuclear layer during late retinal development. In contrast, H3K27 methyltransferase, Ezh2, was highly expressed in the embryonic retina but its expression decreased rapidly after birth. Jmjd3 loss of function in the developing retina resulted in failed differentiation of PKC-positive bipolar cell subsets (rod-ON-BP) and reduced transcription factor *Bhlhb4* expression, which is critical for the differentiation of rod-ON-BP cells. Overexpression of *Bhlhb4*, but not of other BP cell-related genes, such as transcription factors *Neurod* and *Chx10*, in Jmjd3-knockdown retina rescued loss of PKC-positive BP cells. Populations of other retinal cell subsets were not significantly affected. In addition, proliferation activity and apoptotic cell number during retinal development were not affected by the loss of Jmjd3. Levels of histone H3 trimethyl Lys27 (H3K27me3) in the *Bhlhb4* locus were lower in Islet-1–positive BP cells and amacrine cells than in the Islet-1–negative cell fraction. The Islet-1–negative cell fraction consisted mainly of photoreceptors, suggestive of lineage-specific demethylation of H3K27me3 in the *Bhlhb4* locus. We propose that lineage-specific H3K27me3 demethylation of critical gene loci by spatiotemporal-specific Jmjd3 expression is required for appropriate maturation of retinal cells.**

histone methylation | progenitor | interneuron

Methylation of basic amino acid residues in histone is an important epigenetic mechanism to regulate gene expression. Recent studies have shown that histone lysine methylation regulates gene expression by influencing the accessibility of promoter or enhancer regions to transcriptional molecules (1). Di- and trimethylation of lysine 27 on histone H3 (H3K27me2/3) by the histone methyltransferase enhancer of the zeste homolog 2 (Ezh2/Kmt6) with polycomb repressive complex 2 (PRC2) is known as a mechanism of gene repression (2–4). Histone H3 trimethyl Lys27 (H3K27me3) represses gene expression by recruiting PRC1, which recognizes H3K27me3 and ubiquitinate lysine 119 on histone H2A (5). The role of H3K27me3 markers is well established in developmental processes (6). Dynamic switches in polycomb targets that restrict pluripotency and define the developmental potential of progenitor cells have been demonstrated by differentiation of ES cells into Pax6-positive radial-glial neuronal progenitor cells (7). The role of H3K27 in defining the timing of neurogenesis and gliogenesis was shown in cortical neurons by ablating Ezh2 at different developmental stages (8–10). Jmjd3 (Kdm6b) and Utx (Kdm6a) are H3K27 demethylases (11, 12). Jmjd3 is required to regulate the maintenance of the respiratory rhythm generator during late development and in the function of neuronal networks (13).

The vertebrate neural retina is organized into a laminar structure composed of six types of neurons and glial cells. In the mouse, these major retinal cell classes are generated from retinal progenitor cells between embryonic day (E) 11 and postnatal day (P) 10 in a conserved temporal order (14). The importance of histone methylation during retinal development has been discussed in previous studies (details are provided in *SI Note 1*). Recently, it was reported that loss of function of *ezh2* in *Xenopus* causes defective proliferation of retinal progenitor cells and repression of proneural gene expression (15). *Xenopus ezh2* was expressed in the ganglia cell layer (GCL) and inner nuclear layer (INL) in the developing retina, and low-level expression of *jmjd3* in these layers has been reported (16). However, the functional roles of the H3K27 markers in mammalian retinal development have not been reported. In the present study, we examined the roles of H3K27 markers in retinal cell differentiation by ablating Jmjd3 during retinal development. We show that timed *Jmjd3* expression, which results in the demethylation of key genes and retinal maturation factors, plays a critical role in the differentiation of retinal subsets.

## Results

**Jmjd3 Expression in the INL of Developing Retina.** We first examined the expression patterns of enzymes related to H3K27 modification. Only one enzyme (Ezh2) is known to act as a methyltransferase, whereas three enzymes (Jmjd3, Utx, and Uty) are demethylases at the H3K27 site (17). We examined the expression patterns of Jmjd3 and Utx in the developing mouse retina using in situ hybridization (Fig. 1 *A* and *B* and Fig. S1 *A* and *B*). *Jmjd3* was expressed as early as E15 in the retina, and a weak signal was observed in the inner half of

### Significance

The role of repressive gene regulation through histone modifications is known in various biological processes. Histone H3 trimethyl Lys27 (H3K27me3) represses gene expression, and our goal was to understand how this methylation regulates cell differentiation in the vertebrate retina. In this work, we focused on the role of demethylase (Jmjd3) of H3K27me3 in retinal development. Spatiotemporal expression patterns of Jmjd3 during retinal development were shown. Suppression of Jmjd3 expression during retinal development resulted in the failure of differentiation of retinal cell subsets. Lowered expression of genes essential for differentiation of the subsets by loss of expression of Jmjd3 was observed. Therefore, we propose that lineage-specific H3K27me3 demethylation of critical gene loci by spatiotemporal-specific Jmjd3 expression is required for appropriate maturation of retinal cells.

Author contributions: H. Kuribayashi, S.S., and S.W. designed research; A.I., T.I., H. Kuribayashi, S.S., Y.M., and Y.B. performed research; H.N., T.F., H. Koseki, and A.M. contributed new reagents/analytic tools; A.I., T.I., and S.W. analyzed data; and S.W. wrote the paper.

The authors declare no conflict of interest.

This article is a PNAS Direct Submission. S.B. is a guest editor invited by the Editorial Board.

[1]To whom correspondence should be addressed. E-mail: sumiko@ims.u-tokyo.ac.jp.

This article contains supporting information online at www.pnas.org/lookup/suppl/doi:10.1073/pnas.1311480111/-/DCSupplemental.

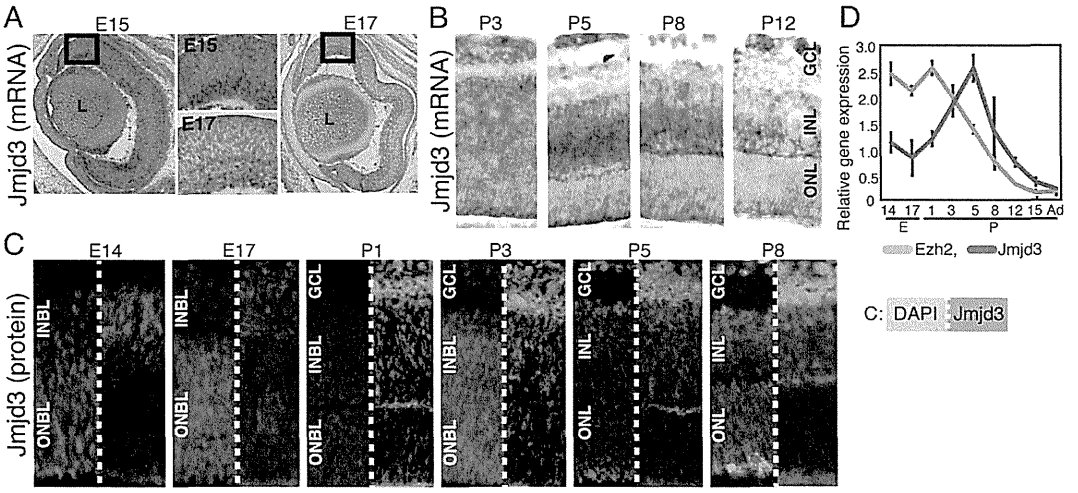


**Fig. 1.** Expression of Jmjd3 and Ezh2 in developing retina. In situ hybridization (*A* and *B*) and immunostaining (*C*) of *Jmjd3* in the developing mouse retina. Mouse retinas at indicated developmental stages were frozen-sectioned, and in situ hybridization and immunostaining were done. Signals in *A* and *B* are visualized using the 5-Bromo-4-chloro-3-indolyl phosphate (BCIP) and nitro-blue tetrazolium chloride (NBT) system. In *C*, Jmjd3 signals are shown in green and gray signals show nuclear staining by DAPI. (*D*) Expression of mRNA of *Jmjd3* and *Ezh2* was examined by RT-qPCR using total RNA extracted from the retina at different developmental stages. An average of three independent samples is shown with the SD. Ad, adult; L, lens; ONBL, outer neuroblastic layer.

the retina. At E17 and P3, the *Jmjd3* signal was weak and the region of expression was difficult to identify (Fig. 1 *A* and *B*). At P5, a signal was observed in the INL and GCL. At P8 and P12, signals in the INL decreased, although a faint signal was still detected (Fig. 1*B*). The *Utx* in situ hybridization signal was very weak, and at P8 and P12, faint signals were observed in the INL (Fig. S1*A*, arrows). Hybridization analysis with sense probes targeting *Jmjd3* gave relatively high background but did not generate specific signals, and probes for *Utx* gave no background or specific signals for the examined stages (Fig. S1*B*). We then performed immunostaining of Jmjd3 with retinal markers. At E14 and E17, Jmjd3 was expressed in GCL and at the inner side of the blastic layer (Fig. 1*C*). Costaining with the Ki67 proliferation antigen indicated that Jmjd3 was expressed in postmitotic cells (Fig. S1*C*). At P1, Jmjd3 was weakly expressed in GCL, and at P3, signals appeared at the inner neuroblastic layer (INBL) (Fig. 1*C*). At P5, the Müller glia marker Ccdn3 (P5) and pan-bipolar (BP) marker Chx10 (P5 and P8) colocalized with Jmjd3, but PNR (Nr2e3), which marks rod photoreceptors (18), did not in P5 and P8 (Fig. S1*C*). RT-quantitative PCR (qPCR) showed that *Jmjd3* expression peaked at the P5 retina, and was relatively low before and after this stage (Fig. 1*D*). Ezh2 is known to be highly expressed in the retina in the INBL at E16 but is undetectable in adult retina (19). RT-qPCR showed that the level of *Ezh2* decreased after birth, and when retinal development was complete at about 2 wk after birth, *Ezh2* expression was negligible (Fig. 1*D*). Immunostaining showed that Ezh2 was expressed in the whole retinal area at E14 and in all layers (GCL, INL, and outer neuroblastic layer) at E17 (Fig. S1*D*). At P5, Ezh2 was expressed in the GCL and weakly in some INL cells. At P8, expression of Ezh2 was observed in the outer half of the INL.

**Jmjd3 Knockdown in the Developing Retina Results in Loss of Rod-ON-BP Cells.** To examine the role of demethylation of H3K27 in retinal development, we performed Jmjd3 loss-of-function analysis. At E17, the retina was transfected with U6 promoter-driven shRNA for *Jmjd3* (sh-Jmjd3) with an EGFP expression plasmid and cultured as explants. We first examined the effects of sh-Jmjd3 on H3K27me3 in the retina. Immunostaining (Fig. S2*A*) showed that the patterns of H3K27me3 in the developing retina were comparable to those in previous reports (20). Next, the effects of sh-Jmjd3 on the H3K27me3 expression pattern were examined. At day 5, signals with stronger intensity for H3K27me3, especially in the INL, were observed in sh-Jmjd3 transfected retina compared with sh-control transfected samples (Fig. S2*B*). At day 10, signal intensity was slightly stronger in the outer nuclear layer (ONL) (Fig. S2*C*). In the control, H3K27me3 signals were observed in the INL but very weakly in the ONL. However, in sh-Jmjd3–expressing retina, similar expression levels in the ONL and INL were observed (Fig. S2*D*). Quantification of H3K27me3-positive cells showed a higher number of positive cells in sh-Jmjd3–expressing samples than in sh-control samples at 5, 10, and 14 d of culture (Fig. S2*E*). We next examined retinal progenitor cell differentiation in the absence of Jmjd3 after 14 d of culture. The gross morphology of the three-layer structure of the sh-Jmjd3–expressing retina was maintained, and we examined the differentiation patterns of the retinal cell subtypes based on immunostaining. Initially, we focused on the differentiation of cells localized to the INL, because Jmjd3 was mainly expressed in the INL. Chx10 is a pan-BP marker, and the number of Chx10-positive cells in the sh-Jmjd3–expressing retina was slightly lower than in the control (Fig. 2 *A* and *E*). PKC is a marker of rod-ON-BP cells, and PKC-positive cells were almost completely absent from retinas transfected with sh-Jmjd3 (Fig. 2 *B* and *E*). Bhlhb5 is a marker of cone-OFF-BP cells and GABAergic amacrine cells, and we detected an increase in the number of displaced amacrine cells in the GCL (Fig. 2*C*, green arrows and Fig. 2*E*). In the INL, amacrine and BP cells were not clearly distinguished, and the total number of Bhlhb5-positive cells in the INL was comparable (Fig. 2*E*). Cone-OFF-BP cells normally express Recoverin, as seen in the control retina at the border of the ONL and INL (Fig. 2*D*, yellow arrows). However, Recoverin-positive Cone-OFF-BP cells were not detected in sh-Jmjd3–transfected retina (Fig. 2*E*). Recoverin expression in the ONL was observed in rod photoreceptors as expected (Fig. 2*D*). Isl1 is a marker of rod and cone-ON-BP and cholinergic amacrine cells (21, 22). The number of Isl1-positive ON-BP cells decreased by about 20% in sh-Jmjd3–transfected retina (Fig. S3*A*, yellow arrows and Fig. 2*F*). Because PKC-positive cells are a subset of Isl1-positive cells, the decrease in Isl1-positive cells likely corresponded to a decrease in PKC-positive cells. In contrast, the number of Isl1-positive amacrine cells in the INL and of displaced amacrine cells was comparable to that of the control (Fig. 2*F*). HuC/D is a marker of amacrine cells, and the number of displaced amacrine cells was increased in the sh-Jmjd3–transfected retina (Fig. S3*B*, yellow arrows), suggesting that

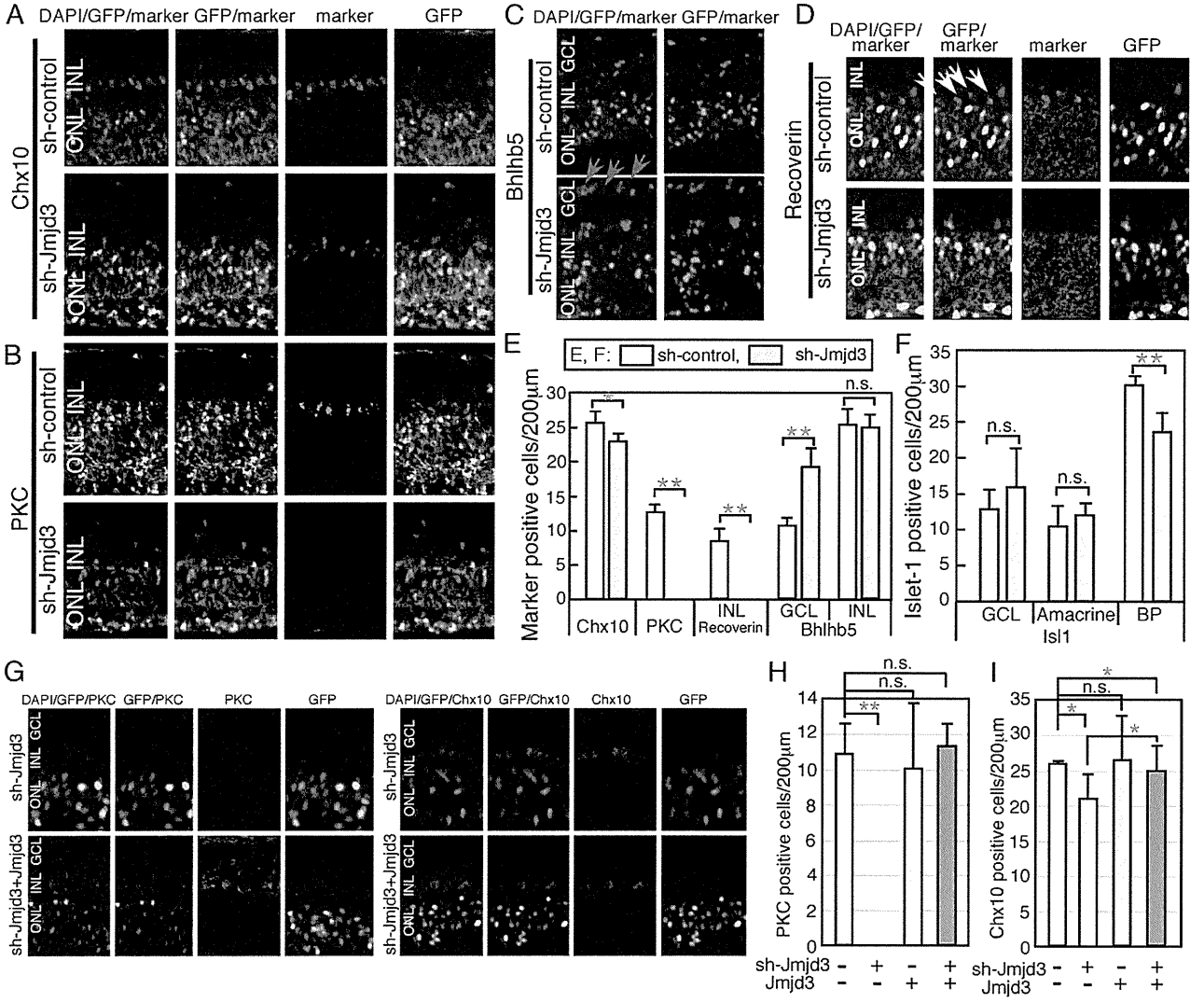


**Fig. 2.** Knockdown of Jmjd3 expression during retinal development. Plasmids encoding CAG-EGFP/U6-shRNA-Jmjd3 (sh-Jmjd3)/control U6 (sh-control) (*A–D*), or CAG-EGFP/sh-Jmjd3/Jmjd3 expression plasmid (*G–I*) were introduced into the retina (E17) by electroporation. After 2 wk of explant culture, the retina was frozen-sectioned and immunostained using antibodies to antiretinal subset markers as indicated. In *E*, *F*, *H*, and *I*, the number of marker-positive cells in the electroporated region (200 μm) as judged by EGFP fluorescence was counted in sections. Green arrows in *C* indicate displaced amacrine cells, and yellow arrows in *D* indicate cone-OFF-BP cells. More than five sections from three independent samples were counted, and values with SDs are shown. $^{**}P < 0.01$, $^{*}P < 0.05$, and $P > 0.05$ (n.s.) were calculated by the Student *t* test. n.s., not significant.

Isl1-positive and HuC/D-positive displaced amacrine cells are at least partially different populations. We obtained similar results using a second *Jmjd3* shRNA. The number of other cell types, such as Müller glia [glutamine synthetase (GS)], rod photoreceptors, and retinal ganglion cells (RGCs), were comparable to those of the control samples (Fig. S3 *C–E* and *G*). Neurite extension of RGCs was also comparable between control and sh-Jmjd3–expressing retina (Fig. S3*F*). We then examined the proliferation and apoptosis of retina expressing sh-Jmjd3 by examining BrdU incorporation, as well as the expression of Ki67 and active caspase-3 (Fig. S4). We transfected sh-Jmjd3 at two different retina developmental stages (E14 and E17), and we examined proliferation and apoptosis at six time points (Fig. S4*A*). The number of active caspase-3–positive cells at E17~10 d showed a slightly but statistically significant difference, but no other samples showed significant differences between control and sh-Jmjd3–expressing retina (Fig. S4 *B–E*).

We then examined cotransfection of *Jmjd3* expression plasmids and sh-Jmjd3, and found that expression of Jmjd3 in the sh-Jmjd3–transfected retina recovered expression of PKC (Fig. 2 *G* and *H*) and Chx10 (Fig. 2 *G* and *I*). Therefore, we identified specific loss of PKC-positive rod-ON-BP cells and Recoverin-positive cone-OFF-BP cells as a consequence of Jmjd3 down-regulation.

**Decreased Expression of Bhlhb4 and Vsx1 Due to Suppression of Jmjd3 Expression.** We explored whether expression of BP cell differentiation-related genes was affected by Jmjd3 down-regulation. A plasmid encoding sh-Jmjd3 was introduced into the retina at E15 and was cultured for 12 d. The expression levels of various genes were then examined by RT-qPCR (Fig. 3*A*). As expected, *Jmjd3* expression significantly decreased. *Bhlhb4* is essential for the maturation of rod-ON-BP cells, which were labeled for PKC (23), and *Vsx1* plays a pivotal role in the differentiation of cone-OFF-BP

cells, which were marked by Recoverin (24). We found that the expression levels of *Bhlhb4* and *Vsx1* were strongly suppressed in the presence of sh-Jmjd3 (Fig. 3*A*). Therefore, the loss of PKC-positive rod-ON-BP cells and Recoverin-positive cone-OFF-BP cells may be explained by suppressing the expression of Bhlhb4 and Vsx1, respectively, by sh-Jmjd3. The expression levels of *Chx10*, *Og9x*, and *Isl1* were lower in the sh-Jmjd3–expressing cells (Fig. 3*A*), whereas difference of expression of the remaining genes between control and sh-Jmjd3–expressing samples was not statistically significant.

Using qPCR, we examined the transition of *Bhlhb4* and *Vsx1* expression during retinal development using whole retinas at various developmental stages. *Bhlhb4* and *Vsx1* expression was not detectable until P5, and their expression levels increased markedly with retinal development (Fig. 3*B*).

We next determined the levels of H3K27me3 at the *Bhlhb4*, *Vsx1*, and other BP-related gene loci in BP cells. To obtain retinal cells enriched for BP cells, we used Isl1, which is a marker of rod- and cone-ON-BP and cholinergic amacrine cells (21, 22). We stained permeabilized retinal cells at P9 with an anti-Isl1 antibody, followed by staining with a secondary antibody conjugated with phycoerythrin. The Isl1-positive and Isl1-negative cells were then purified using a cell sorter (Fig. S5 *A* and *B*), and ChIP analysis using an anti-H3K27me3 antibody was performed. The H3K27me3 level at the *Bhlhb4* and *Vsx1* loci was lower in Isl1-positive cells than in Isl1-negative cells (Fig. 3*C*). Because Vsx1 is also expressed in type 7 cone-ON-BP cells (24, 25), it is possible that differentiation of type 7 cone-ON-BP cells was defective in sh-Jmjd3–expressing retina. However, this was difficult to confirm, given the lack of a specific marker for this BP subset. Furthermore, although Isl1 is strictly expressed in the ON-BP subset in the mature retina (21, 22, 26), Isl1-KO mice also have OFF-BP subset defects, suggesting that Isl1 is transiently expressed in OFF-BP cell precursors (27) and that the precursors of Recoverin-positive cells are found in the Isl1-positive fractions. The level of H3K27me3 at the *Cdkn2a* (*Ink4a*) locus was not significantly different between the Isl1-positive and Isl1-negative populations, and that at the *Elavl3* locus was slightly higher in Isl1-positive cells. The H3K27me3 level at the *Mash1* locus was significantly lower in Isl1-positive cells (Fig. 3*C*). All other genes showed higher values in Isl1-positive cells than in Isl1-negative cells, but the difference was not statistically significant (Fig. S5*C*). We also examined levels of H3K27me3 at the *Chx10*, *Neurod*, and *GS* loci, but we could not detect reliable qPCR signals because the H3K27me3 levels at these gene loci were too low in both cell fractions.

We then explored whether the pattern of H3K27 levels in the *Bhlhb4* locus is specific for H3K27me3 by examining Histone H3 trimethyl Lys4 (H3K4me3) levels. ChIP analysis of H3K4me3 using Isl1-positive/negative retinal cells at P9 was performed. Interestingly, H3K4me3 marker in the *Bhlhb4* locus was much higher in the Isl1-positive fraction than in the Isl1-negative fraction (Fig. 3*D*), suggesting that H3K4me3 modification also contributes to specific up-regulation of *Vsx1* and *Bhlhb4* in cells

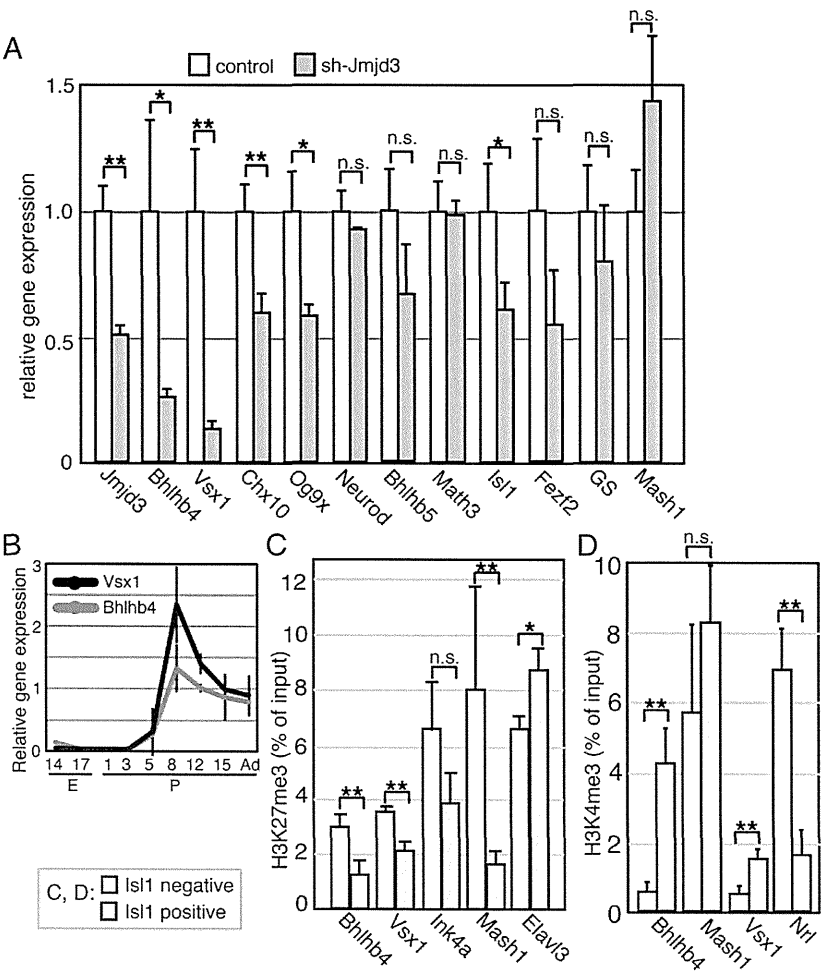


**Fig. 3.** Molecular signatures in sh-Jmjd3–transfected retina. (*A*) Plasmids encoding sh-Jmjd3 or sh-control with CAG-EGFP were introduced into the retina at E15; the retina was then cultured for 12 d as retinal explants, and RT-qPCR was performed. All values of qPCR were normalized by the normalization factor value calculated by housekeeping genes, *Gapdh* and *Sdha*. (*B*) Transition of expression of *Bhlhb4* and *Vsx1* was examined by RT-qPCR during retinal development. H3K27me3 (*C*) or H3K4me3 (*D*) modification of gene loci in purified Isl1-positive or Isl1-negative cells was examined by ChIP analysis. Experiments were done three times independently, and the average and SD are shown. Abcam antibody (ab6002) for H3K27me3 was used in *C*. $^{**}P < 0.01$, $^{*}P < 0.05$, and $P > 0.05$ (n.s.) were calculated by the Student *t* test.

in the Isl1-positive cell fraction. The H3K4me3 level of the *Vsx1* locus was also higher in the Isl1-positive fraction, but that of *Nrl*, which is a photoreceptor-specific gene (28), was higher in Isl1-negative cells (Fig. 3*D*).

**Bhlhb4 Expression Reverses the Loss of PKC-Positive Cells in sh-Jmjd3–Transfected Cells.** We then focused on the PKC-positive BP cells for a more detailed molecular analysis. We investigated whether Bhlhb4 caused the loss of PKC-positive cells in sh-Jmjd3–expressing retina by forcing Bhlhb4 expression in sh-Jmjd3–expressing cells. We first examined the effects of Bhlhb4 expression alone in retinal progenitor cells (Fig. 4 *A–D*). Bhlhb4-expressing and EGFP-expressing plasmids were transfected into the retina at E17, and the retina was cultured as an explant for 2 wk. Differentiation of the retina was then examined by immunostaining of frozen sections (Fig. 4 *A* and *B*). Forced Bhlhb4 expression did not cause apparent morphological abnormalities of the retina, and PKC immunostaining showed comparable differentiation of rod-ON-BP cells (Fig. 4 *A* and *C*). The Bhlhb4-expressing and sh-Jmjd3–expressing plasmids were then cotransfected into E17 retina. Bhlhb4 expression reversed the loss of PKC-positive cells by sh-Jmjd3 (Fig. 4 *A* and *C*), suggesting that the loss of PKC-positive cells by sh-Jmjd3 was caused by the loss of Bhlhb4 expression. The slight decrease in the number of Isl1-positive BP cells caused by sh-Jmjd3 was reversed by Bhlhb4 expression (Fig. 4 *B* and *D*). We also performed rescue experiments using Neurod and Chx10, but we did not observe PKC-positive cells by expressing Neurod or Chx10 in the presence of sh-Jmjd3 (Fig. 4 *E* and *F*).

## Discussion

In the present study, we examined the role of H3K27me3 modification in retinal development and analyzed the effects of loss of function of a demethylation enzyme. We observed a critical role of Jmjd3 for the maturation of PKC-positive BP cell subset development. Because H3K27me3 suppresses gene expression (29, 30), our results were indicative of the importance of timed demethylation to activate genes responsible for proper differentiation of BP cell subsets. Down-regulation of *Bhlhb4* and *Vsx1* expression, both of which are critical for BP subset differentiation, occurred in the absence of Jmjd3. Thus, we propose a model in which H3K27 methylation at loci critical for BP cell maturation occurs in retinal progenitor cells, which is retained during differentiation. Timed demethylation of genes in a specific subset of cells (i.e., BP precursor cells) releases the genes from the transcriptionally silent state (Fig. S6). This is strongly supported by our findings of a lower level of H3K27me3 at critical loci in the BP-enriched cell fraction and of Jmjd3 expression in the

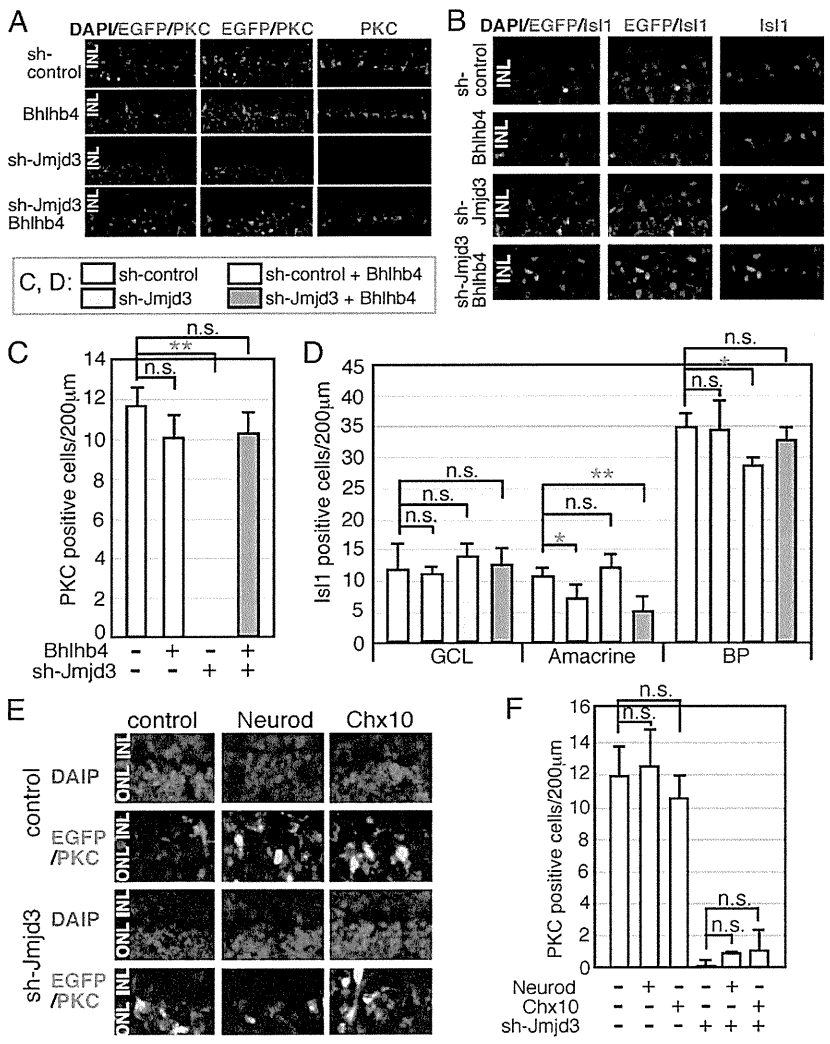


**Fig. 4.** Supplemental expression of Bhlhb4 into sh-Jmjd3–transfected retina. Mouse retina at E17 was isolated, and plasmids encoding CAG-EGFP and sh-Jmjd3 or sh-control with or without CAG-Bhlhb4 (*A–D*) and CAG-Neurod or CAG-Chx10 (*E* and *F*) were introduced into the retina by electroporation. The total amount of transfected plasmids was adjusted as the same for all experiments by the addition of empty vector. (*A*, *B*, and *E*) After 2 wk of explant culture, the retina was frozen-sectioned and immunostained using antibodies to antiretinal subset markers as indicated. (*C*, *D*, and *F*) Number of marker-positive cells in the electroporated region (200 μm) was counted. More than five sections from three independent samples were counted, and values with SDs are shown. $^{**}P < 0.01$, $^{*}P < 0.05$, and $P > 0.05$ (n.s.) were calculated by the Student *t* test.

INL of the postnatal retina. The *Mash1* locus also showed a lower level of H3K27me3 in the BP-enriched cell fraction. Mash1 plays critical roles for BP cell differentiation (31, 32), therefore suggesting that this phenomenon is biologically relevant to achieve cell lineage-specific expression of *Mash1*. However, the mRNA level of *Mash1* in sh-Jmjd3–expressing retina was comparable to that of the control, suggesting some additional mechanisms for regulation of Mash1 transcription.

In contrast to the expression pattern of Jmjd3, H3K27 methyltransferase, *Ezh2* was highly expressed in the embryonic retina. These results suggest that both methylation and demethylation are based on the spatiotemporal dynamics of related enzyme expression patterns. Regulation of the expression pattern dynamics of critical genes for neural fate determination by polycomb and timed H3K27 demethylation in the CNS were suggested previously (7, 10). Furthermore, critical roles for Jmjd3 during early neural development in ES cell neurulation and chick spinal cord development have been demonstrated (33, 34). Our results suggest that during retinal differentiation, Jmjd3 directs differentiation of subsets of neurons to regulate neuron/glia cell fate. During the late phase of neural development, Jmjd3 is required in the embryonic respiratory neuronal network (13). In the immune system, Jmjd3 is induced by bacterial products and inflammatory cytokines, and it is essential for M2 macrophage polarization in response to helminth infection and chitin, which is mediated by Irf4 (35, 36). In addition, Jmjd3 is essential for proper bone marrow macrophage differentiation (36), which suggests that the important role of timed Jmjd3 expression for the maturation of specific cell subsets applies to the hematopoietic system.

We found an increased number of displaced amacrine cells (HuC/D- or Bhlhb5-positive cells) in sh-Jmjd3–treated retina. These cells are the result of failed maturation of PKC-positive BP precursor cells, although the molecular basis for this phenomenon remains unknown. The presence of other Jmjd3 targets in the retina is currently being explored. ChIP sequencing using a purified subfraction of retinal cells could be used to identify Jmjd3 targets, although refinement of the ChIP technique is required to generate reliable results from such a low number of cells. In this study, we used retinal explants in combination with sh-RNA–mediated gene suppression. This system provides an excellent model system for molecular analysis but is limited, because we cannot analyze the effects of sh-RNA on early-born retinal subsets. Because Jmjd3 was strongly expressed in the GCL, it may play a role in the development of RGCs and amacrine cells. This could be addressed by analyzing conditional KOs of Jmjd3 in the future.

## Materials and Methods

All animal experiments were approved by the Animal Care Committee of the Institute of Medical Science, University of Tokyo, and conducted in accordance with the Association for Research in Vision and Ophthalmology statement for the use of animals in ophthalmic and vision research. The U6 promoter driving the shRNA vector was used for targeting Jmjd3, and the pCAG vector was used for overexpression. Plasmids were introduced into retinal explants by electroporation. Frozen sections in optimal cutting temperature compound were used for immunostaining. ChIP-qPCR and RT-qPCR results were normalized in accord with minimum information for publication of quantitative real-time PCR experiment guidelines. Further details are described in *SI Materials and Methods*.

**ACKNOWLEDGMENTS.** We thank Eli Lyons for language assistance and Honami Watanabe for technical advice. This work is supported by a grant-in-aid from the Ministry of Education, Culture, Sports, Science, and Technology of Japan.

1. Kooistra SM, Helin K (2012) Molecular mechanisms and potential functions of histone demethylases. *Nat Rev Mol Cell Biol* 13(5):297–311.
2. Hansen KH, et al. (2008) A model for transmission of the H3K27me3 epigenetic mark. *Nat Cell Biol* 10(11):1291–1300.
3. Margueron R, et al. (2009) Role of the polycomb protein EED in the propagation of repressive histone marks. *Nature* 461(7265):762–767.
4. Cao R, Zhang Y (2004) The functions of E(Z)/EZH2-mediated methylation of lysine 27 in histone H3. *Curr Opin Genet Dev* 14(2):155–164.
5. Morey L, Helin K (2010) Polycomb group protein-mediated repression of transcription. *Trends Biochem Sci* 35(6):323–332.
6. Ringrose L, Paro R (2007) Polycomb/Trithorax response elements and epigenetic memory of cell identity. *Development* 134(2):223–232.
7. Mohn F, et al. (2008) Lineage-specific polycomb targets and de novo DNA methylation define restriction and potential of neuronal progenitors. *Mol Cell* 30(6):755–766.
8. Hirabayashi Y, et al. (2009) Polycomb limits the neurogenic competence of neural precursor cells to promote astrogenic fate transition. *Neuron* 63(5):600–613.
9. Pereira JD, et al. (2010) Ezh2, the histone methyltransferase of PRC2, regulates the balance between self-renewal and differentiation in the cerebral cortex. *Proc Natl Acad Sci USA* 107(36):15957–15962.
10. Testa G (2011) The time of timing: How Polycomb proteins regulate neurogenesis. *Bioessays* 33(7):519–528.
11. Agger K, et al. (2007) UTX and JMJD3 are histone H3K27 demethylases involved in HOX gene regulation and development. *Nature* 449(7163):731–734.
12. Jepsen K, et al. (2007) SMRT-mediated repression of an H3K27 demethylase in progression from neural stem cell to neuron. *Nature* 450(7168):415–419.
13. Burgold T, et al. (2012) The H3K27 demethylase JMJD3 is required for maintenance of the embryonic respiratory neuronal network, neonatal breathing, and survival. *Cell Rep* 2(5):1244–1258.
14. Marquardt T, Gruss P (2002) Generating neuronal diversity in the retina: One for nearly all. *Trends Neurosci* 25(1):32–38.
15. Aldiri I, Moore KB, Hutcheson DA, Zhang J, Vetter ML (2013) Polycomb repressive complex PRC2 regulates Xenopus retina development downstream of Wnt/β-catenin signaling. *Development* 140(14):2867–2878.
16. Kawaguchi A, Ochi H, Sudou N, Ogino H (2012) Comparative expression analysis of the H3K27 demethylases, JMJD3 and UTX, with the H3K27 methylase, EZH2, in Xenopus. *Int J Dev Biol* 56(4):295–300.
17. Swigut T, Wysocka J (2007) H3K27 demethylases, at long last. *Cell* 131(1):29–32.
18. Kobayashi M, et al. (1999) Identification of a photoreceptor cell-specific nuclear receptor. *Proc Natl Acad Sci USA* 96(9):4814–4819.
19. Rao RC, et al. (2010) Dynamic patterns of histone lysine methylation in the developing retina. *Invest Ophthalmol Vis Sci* 51(12):6784–6792.
20. Popova EY, et al. (2012) Stage and gene specific signatures defined by histones H3K4me2 and H3K27me3 accompany mammalian retina maturation in vivo. *PLoS ONE* 7(10):e46867.
21. Galli-Resta L, Resta G, Tan SS, Reese BE (1997) Mosaics of islet-1-expressing amacrine cells assembled by short-range cellular interactions. *J Neurosci* 17(20):7831–7838.
22. Elshatory Y, Deng M, Xie X, Gan L (2007) Expression of the LIM-homeodomain protein Isl1 in the developing and mature mouse retina. *J Comp Neurol* 503(1):182–197.
23. Bramblett DE, Pennesi ME, Wu SM, Tsai MJ (2004) The transcription factor Bhlhb4 is required for rod bipolar cell maturation. *Neuron* 43(6):779–793.
24. Chow RL, et al. (2004) Control of late off-center cone bipolar cell differentiation and visual signaling by the homeobox gene Vsx1. *Proc Natl Acad Sci USA* 101(6):1754–1759.
25. Shi Z, et al. (2011) Vsx1 regulates terminal differentiation of type 7 ON bipolar cells. *J Neurosci* 31(37):13118–13127.
26. Haverkamp S, Ghosh KK, Hirano AA, Wässle H (2003) Immunocytochemical description of five bipolar cell types of the mouse retina. *J Comp Neurol* 455(4):463–476.
27. Elshatory Y, et al. (2007) Islet-1 controls the differentiation of retinal bipolar and cholinergic amacrine cells. *J Neurosci* 27(46):12707–12720.
28. Swaroop A, et al. (1992) A conserved retina-specific gene encodes a basic motif/leucine zipper domain. *Proc Natl Acad Sci USA* 89(1):266–270.
29. Müller J, et al. (2002) Histone methyltransferase activity of a Drosophila Polycomb group repressor complex. *Cell* 111(2):197–208.
30. Czermin B, et al. (2002) Drosophila enhancer of Zeste/ESC complexes have a histone H3 methyltransferase activity that marks chromosomal Polycomb sites. *Cell* 111(2): 185–196.
31. Pollak J, et al. (2013) ASCL1 reprograms mouse Muller glia into neurogenic retinal progenitors. *Development* 140(12):2619–2631.
32. Gamm DM, et al. (2008) Regulation of prenatal human retinal neurosphere growth and cell fate potential by retinal pigment epithelium and Mash1. *Stem Cells* 26(12): 3182–3193.
33. Akizu N, Estarás C, Guerrero L, Martí E, Martínez-Balbás MA (2010) H3K27me3 regulates BMP activity in developing spinal cord. *Development* 137(17):2915–2925.
34. Burgold T, et al. (2008) The histone H3 lysine 27-specific demethylase Jmjd3 is required for neural commitment. *PLoS ONE* 3(8):e3034.
35. De Santa F, et al. (2007) The histone H3 lysine-27 demethylase Jmjd3 links inflammation to inhibition of polycomb-mediated gene silencing. *Cell* 130(6):1083–1094.
36. Satoh T, et al. (2010) The Jmjd3-Irf4 axis regulates M2 macrophage polarization and host responses against helminth infection. *Nat Immunol* 11(10):936–944.

HEPATOLOGY
Official Journal of the American Association for the Study of Liver Diseases

NEW HORIZONS

# Liver Regeneration by Stem/Progenitor Cells

Tohru Itoh and Atsushi Miyajima

**The liver is renowned for its strong, robust regenerative capacity, employing different modes of regeneration according to type and extent of injury. The process of compensatory hypertrophy of the liver upon partial hepatectomy has been standing as a classical model for studying organ regeneration in mammals and a subject of exhaustive analyses. Meanwhile, in view of the physiological relevance for many of the human liver pathologies induced upon toxic insults or hepatitis, other injury models have recently drawn increasing attention. In those damaged livers where hepatocyte proliferation is compromised, adult liver stem/progenitor cells (LPCs) are activated and differentiate to hepatocytes and cholangiocytes, leading to functional recovery of the organ. Here, we summarize and discuss recent findings on the mechanisms underlying the regeneration process of the liver. Whereas the primary focus of this article is on those related to LPC-mediated regeneration, we also introduce topics on compensatory hypertrophy, where application of new technologies and molecular genetics approaches in mice has gained a paradigm shift. Identification of various markers for LPC populations has expedited their characterization and enabled us to examine their differentiation potential *in vivo* using genetic lineage-tracing approaches. Comprehensive studies regarding intercellular signaling pathways and their modes of action have succeeded in elucidating novel frameworks for the LPC-niche interaction functioning in the regenerating liver. *Conclusion*: Advancing our understanding of the cellular and molecular mechanisms for liver regeneration should provide a basis for developing therapeutic strategies to treat patients with liver disease. (HEPATOLOGY 2014;59:1617-1626)**

The liver is a vital organ to maintain systemic homeostasis, playing multiple important biological functions, such as nutrient metabolism, detoxification, serum protein synthesis, bile secretion, and immune regulation. It receives blood flow from the intestine through the portal vein, through which various types of substances, including toxins, drugs, and xenobiotics, can be brought. Thus, the liver can be regarded as the primary barrier or filter in the body and is inherently subject to damages caused by these compounds. In addition, it can be targeted by several kinds of hepatotropic viruses, leading to acute or chronic injury. To encounter these potential damages and adequately exert its functions, the liver has extremely high potential for regeneration.

Two modes of liver regeneration have been known (Fig. 1). In regeneration after surgical removal of a portion of the liver (partial hepatectomy; PHx), the remaining hepatocytes and other liver cells are not injured. In this case, it has been generally considered that regeneration can be achieved by the simple proliferation of remaining cells, with each cell type showing different kinetics in proliferation.[1] Upon PHx, hepatocytes are the first to enter cell cycle and their DNA synthesis peaks at approximately 20-24 hours postoperation in rats, whereas the other cell types proliferate later. In particular, regrowth of the intrahepatic biliary tree occurs through proliferation of remaining bile duct epithelial cells (BECs; or cholangiocytes) and

*Abbreviations: 2-AAF, 2-acetylaminofluorene; BECs, bile duct epithelial cells; BM, bone marrow; CDE, choline-deficient, ethionine-supplemented; CK19, cytokeratin-19; DDC, 3,5-diethoxycarbonyl-1,4-dihidro-collidine; EpCAM, epithelial cell adhesion molecule; FCM, flow cytometry; FGF, fibroblast growth factor; Foxl1, forkhead box protein L1; HGF, hepatocyte growth factor; HpSCs, hepatic stem cells; HSCs, hepatic stellate cells; KI, knock-in; KO, knockout; Lgr5, leucine-rich repeat-containing G protein-coupled receptor 5; LPCs, liver stem/progenitor cells; mAb, monoclonal antibody; MFs, myofibroblasts; PHx, partial hepatectomy; α-SMA, alpha-smooth muscle actin; Sox9, SRY (sex-determining region Y)-box 9; Tg, transgenic; Thy1, thymus cell antigen 1; TNF, tumor necrosis factor; TWEAK, TNF-related WEAK inducer of apoptosis.*

*From the Laboratory of Cell Growth and Differentiation, Institute of Molecular and Cellular Biosciences, The University of Tokyo, Tokyo, Japan.*

*Received July 3, 2013; accepted September 11, 2013.*

*Address reprint requests to: Tohru Itoh, Ph.D., Laboratory of Cell Growth and Differentiation, Institute of Molecular and Cellular Biosciences, The University of Tokyo, Yayoi, Bunkyo-ku, Tokyo 113-0032, Japan. E-mail: itohru@iam.u-tokyo.ac.jp; fax: +81-3-5841-8475.*



*View this article online at wileyonlinelibrary.com.*
*DOI 10.1002/hep.26753*
*Potential conflict of interest: Nothing to report.*